Using ice core measurements from Taylor Glacier, Antarctica to calibrate *in situ* cosmogenic ^{14}C production rates by muons

Michael N. Dyonisius[1,2], Vasilii V. Petrenko[1], Andrew M. Smith[3], Benjamin Hmiel[1,a], Peter Neff[4,1], Bin Yang[3], Quan Hua[3], Jochen Schmitt[5], Sarah A. Shackleton[6,b], Christo Buizert[7], Philip F. Place[1,c], James A. Menking[7,d], Ross Beaudette[6], Christina Harth[6], Michael Kalk[7], Heidi Roop[4], Bernhard Bereiter[6], Casey Armanetti[7,e], Isaac Vimont[8,f], Sylvia Englund Michel[8], Edward J. Brook[7], Jeffrey P. Severinghaus[6], Ray F. Weiss[6], Joseph R. McConnell[9]

[1]Department of Earth and Environmental Sciences, University of Rochester, NY 14627, USA
[2]Physics of Ice, Climate and Earth, Niels Bohr Institute, University of Copenhagen, Copenhagen 2200, Denmark
[3]Centre for Accelerator Science (CAS), Australian Nuclear Science and Technology Organization (ANSTO), Lucas Heights, NSW 2234, Australia
[4]Department of Soil, Water, and Climate, University of Minnesota, Saint Paul, MN 55108, USA.
[5]Climate and Environmental Physics, Physics Institute and Oeschger Centre for Climate Change Research, University of Bern, CH-3012 Bern, Switzerland.
[6.] Scripps Institution of Oceanography (SIO), University of California, San Diego, La Jolla, CA 92037, USA.
[7.] College of Earth, Ocean and Atmospheric Sciences, Oregon State University, Corvallis, OR 97331, USA.
[8.] Institute of Arctic and Alpine Research, University of Colorado Boulder, Boulder, CO 80303, USA
[9.] Desert Research Institute, Reno, NV 89512, USA

Present address
[a.] Environmental Defense Fund, Austin, TX, USA
[b.] Department of Geosciences, Princeton University, Princeton, NJ 08544, USA.
[c.] School of Marine and Atmospheric Sciences, Stony Brook University, Stony Brook, NY, USA
[d.] Australian Antarctic Program Partnership, University of Tasmania, Australia
[e.] Graduate School of Design, Harvard University
[f.] National Oceanic and Atmospheric Administration, Global Monitoring Division, Boulder, CO, USA

Correspondence to: Michael N. Dyonisius (michael.dyonisius@nbi.ku.dk)

Abstract. Cosmic rays entering the Earth's atmosphere produce showers of secondary particles such as neutrons and muons. The interaction of these neutrons and muons with oxygen-16 (^{16}O) in minerals such as ice and quartz can produce carbon-14 (^{14}C). In glacial ice, ^{14}C is also incorporated through trapping of ^{14}C-containing atmospheric gases ($^{14}CO_2$, ^{14}CO, and $^{14}CH_4$). Understanding the production rates of *in situ* cosmogenic ^{14}C is important to deconvolve the *in situ* cosmogenic and atmospheric ^{14}C signals in ice, both of which contain valuable paleoenvironmental information. Unfortunately, the *in situ* ^{14}C production rates by muons (which are the dominant production mechanism at depths of >6 m solid ice equivalent) are uncertain. In this study, we use measurements of *in situ* ^{14}C in ancient ice (>50 kilo-annum before present, ka BP) from the Taylor Glacier, Antarctica ablation site, in combination with a 2D ice flow model to better constrain the compound-specific rates of ^{14}C production by muons and the partitioning of *in situ* ^{14}C between CO_2, CO and

CH4. Our measurements show that 33.7% (±11.4%, 95% confidence interval) of the produced cosmogenic ^{14}C forms ^{14}CO, 66.1% (±11.5%, 95% confidence interval) of the produced cosmogenic ^{14}C forms $^{14}CO_2$. $^{14}CH_4$ represents a very small fraction (< 0.3%) of the total. Assuming that the majority of *in situ* muogenic ^{14}C in ice forms $^{14}CO_2$, ^{14}CO, and $^{14}CH_4$, we also find that the commonly used values for muogenic ^{14}C production rates as determined from laboratory studies with quartz and transferred to ice using nuclear chemistry considerations (Heisinger et al., 2002a, 2002b) are too high by factors of 5.7 (3.6-13.9, 95% confidence interval) and 3.7 (2.0-11.9 95% confidence interval) for negative muon capture and fast muon interactions, respectively. This apparent discrepancy in muogenic ^{14}C production rates in ice and quartz currently lacks a good explanation and requires further investigation.

1. Introduction

1.1. Potential applications of ^{14}C measurements in ice and *in situ* cosmogenic ^{14}C production from ^{16}O in Earth's surface minerals

As snow accumulates on ice sheets, it gradually densifies into firn and ice (Herron and Langway, 1980). During the firn to ice transition, the air in the interstitial space between the ice grains becomes trapped into bubbles within the ice matrix (Buizert, 2013). Included in the paleoatmospheric air trapped in the bubbles are ^{14}C-containing atmospheric gases ($^{14}CO_2$, ^{14}CO, and $^{14}CH_4$) (Fireman and Norris, 1982). ^{14}C in ice is also produced through interactions of secondary cosmic rays with ^{16}O directly in the lattice of the ice grains (i.e., "*in situ*") (Lal et al., 1990). Following the cosmogenic nuclear reactions, the "hot" ^{14}C atom interacts with atoms in the surrounding ice lattice to produce $^{14}CO_2$, ^{14}CO, and $^{14}CH_4$ (Lal et al., 1990; Petrenko et al., 2013).

Both the trapped atmospheric and *in situ* cosmogenic ^{14}C signals in ice have unique applications. For example, the paleoatmospheric component of $^{14}CH_4$ in ice cores has been used to constrain past CH_4 emissions from old carbon reservoirs such as methane hydrates, permafrost, and geologic seeps (Dyonisius et al., 2020; Hmiel et al., 2020; Petrenko et al., 2009, 2017). Paleoatmospheric $^{14}CO_2$ can be potentially used for absolute dating of ice core gases (Andree et al., 1984; Van De Wal et al., 1994) and to improve the radiocarbon calibration curve (Reimer et al., 2020; Hogg et al., 2020) in periods where tree-ring data are not available. Measurements of ^{14}CO in the modern atmosphere have been used to constrain the oxidative capacity of the atmosphere (Brenninkmeijer et al., 1992; Petrenko et al., 2021) and thus, paleoatmospheric ^{14}CO in ice cores can be used for a similar application. The *in situ* cosmogenic component of ^{14}CO at ice core sites can be potentially be used to reconstruct the past cosmic ray flux (BenZvi et al., 2019). Finally, measurements of the *in situ* cosmogenic component of $^{14}CO_2$ and ^{14}CO can be used to constrain the accumulation/ablation rate of the ice core site (e.g., Lal et al., 1990; Lal and Jull, 1990). Unfortunately, the paleoatmospheric and *in situ* cosmogenic components of ^{14}C in ice exist in a combined form and cannot be separated analytically (Petrenko et al., 2016). To separate these signals, it is important to have accurate

estimates of the cosmogenic ^{14}C production rates and the partitioning among the *in situ* produced ^{14}C species ($^{14}CO_2$, ^{14}CO, and $^{14}CH_4$) in ice.

In situ cosmogenic ^{14}C production in ice is analogous to production in quartz because both minerals share the same target atom (^{16}O). Measurements of *in situ* cosmogenic nuclides (^{3}He, ^{10}Be, ^{14}C, ^{21}Ne, ^{26}Al, and ^{36}Cl) in near-surface rocks are commonly used as tools to constrain various Earth surface processes such as the timing of glacial retreat and erosion rates (Gosse and Phillips, 2001; Balco, 2020). Due to its short half-life of 5700 ± 30 yr (Kutschera, 2019), ^{14}C in quartz is uniquely suited to characterize surface processes on millennial timescales (e.g., Spector et al., 2019; Pendleton et al., 2019). *In situ* cosmogenic ^{14}C measurements are also often paired with measurements of longer-lived nuclides such as ^{10}Be and ^{26}Al (e.g., Hippe, 2017; Skov et al., 2019) to study complex surface processes such as subglacial erosion and millennial-scale glacier retreats/re-advances.

In situ cosmogenic ^{14}C in Earth's surface minerals is produced from ^{16}O by 3 nuclear reactions: (1) neutron-induced spallation (Lal and Peters, 1967), (2) negative muon capture (Heisinger et al., 2002b), and (3) interactions with fast muons (Heisinger et al., 2002a). The depth-dependence of the ^{14}C production rate for each mechanism in ice is shown in Fig. 1. Neutron-induced spallation dominates the ^{14}C production at the surface but is quickly attenuated with depth, while the production rates from the two muon mechanisms are lower near the surface but dominate at larger depths. Characterizing the *in situ* cosmogenic ^{14}C production rates from muons is especially important for applications of cosmogenic surface exposure dating where the samples might be exposed to subsurface cosmic-ray flux for an extended period. One example of this would be a bedrock that is covered by a relatively thin (e.g., tens of meters) glacier.

Understanding the muogenic ^{14}C component is especially important for ^{14}C studies in ice. Prior studies have shown that at snow accumulation sites, most of the *in situ* ^{14}C produced in the firn (including the majority of neutron-produced ^{14}C) is lost to the atmosphere via gas movement in the firn open porosity (Petrenko et al., 2013; Van der Kemp et al., 2000; Wilson and Donahue, 1992). *In situ* cosmogenic ^{14}C mainly starts to accumulate in deeper ice where gas exchange with the atmosphere no longer happens and at these depths the ^{14}C production is entirely from the muon mechanisms. Thus, the *in situ* cosmogenic ^{14}C signal in traditional deep ice cores is dominated by production from muons and constraining the muogenic ^{14}C production rates is critical to disentangle the *in situ* cosmogenic and atmospheric ^{14}C signals in ice cores. Unfortunately, the *in situ* ^{14}C production rates by muons in both ice and quartz are still highly uncertain (Hippe, 2017).

The production rates of cosmogenic nuclides are usually determined from calibration sites where independent controls on exposure history are available such as ^{14}C dating from organic materials (e.g., Lifton et al., 2015) or argon ($^{40}Ar/^{39}Ar$) dating from lava flows (e.g., Balbas and Farley, 2020; Fenton et al., 2019). However, the commonly used estimates of muogenic ^{14}C production rates (for both negative muon capture and fast muon reactions) were derived through laboratory irradiation of artificial target compounds (Heisinger

et al., 2002a, 2002b). To our knowledge, there is only one prior study (Lupker et al., 2015) that provided estimates of total muogenic *in situ* ^{14}C production rates based on measurements in a natural setting. Using ^{14}C measurements from a 15.5m deep quartzite core from Leymon High, Spain, Lupker et al. (2015) estimated a sea level high latitude (SLHL) surface production rate of 3.34 (+0.43/-1.07) ^{14}C atoms g^{-1} quartz yr^{-1} for negative muon capture and 0 (+0.42/-0.00) ^{14}C atoms g^{-1} quartz yr^{-1} for fast muon interactions (1σ uncertainties). The large uncertainties on the ^{14}C production rates (especially the production rate from fast muons) estimated by Lupker et al. (2015) were due to relatively large measurement uncertainty for their deepest samples and small contribution to the ^{14}C signal from fast muons. Petrenko et al. (2016) also used ^{14}C measurements (^{14}CO, $^{14}CO_2$, and $^{14}CH_4$) in >50 ka BP ice for the 2 – 20 m depth range from Taylor Glacier, Antarctica to constrain the ^{14}C production rates in ice. The old age of the ice ensured that all in-situ cosmogenic and paleoatmospheric ^{14}C inherited from the ice accumulation site had decayed away. Unfortunately, Petrenko et al. (2016) were unable to accurately constrain the total ^{14}C production rates because of the high uncertainty resulting from the melt-extraction technique used to obtain their $^{14}CO_2$ measurements (see Section 1.3).

1.2. Overview of ^{14}C production from muons

Following Heisinger et al. (2002b), the production rate of ^{14}C (atoms g^{-1} yr^{-1}) by negative muon capture (P_{neg}) as a function of lithospheric depth (h, typically in g cm^{-2}) is given by

$$P_{neg}(h) = R_{\mu^-}(h) \cdot f_{tot} \quad \text{Eq.1}$$

$$f_{tot} = f_C \cdot f_D \cdot f^* \quad \text{Eq.2}$$

where $R_{\mu^-}(z)$ is the stopping rate of negative muons (muons g^{-1} yr^{-1}) at lithospheric depth h and f_{tot} is the overall probability of ^{14}C production in ice from a stopped negative muon (unitless). The stopping rate of negative muons at the given depth $R_{\mu^-}(h)$ has been empirically determined from measurements at deep underground laboratories (Heisinger et al., 2002b). The lithospheric depth (h) is a product of actual depth (z) and density (ρ) of the target mineral (ρ_{ice} = 0.92 g cm^{-3}).

The total probability (f_{tot}) of ^{14}C production from negative muon capture is expressed by the product of the chemical compound factor (f_C) representing the probability that the stopped muon is captured by one of the target atoms (^{16}O in case of ^{14}C production), the probability that the negative muon does not decay in the K-shell before nuclear capture (f_D), and the effective probability for production of cosmogenic nuclide after μ^- capture by the target atom (f*) (Eq.2; Heisinger et al., 2002b; Lupker et al., 2015). All probability (f) terms in Eq.2 are unitless. From experiments involving laboratory irradiation of artificial targets, the overall probability (f_{tot}) for ^{14}C production in ice from negative muon was estimated to be 0.025 ± 0.002 (Heisinger et al., 2002b).

An expression for the production rate of nuclides by fast muon interactions (P_{fast}) as a function of lithospheric depth (h) is given by Heisinger et al. (2002a):

$$P_{fast}(h) = \sigma_0 \cdot \beta\,(h)\ \phi(h) \cdot \bar{E}(h)^{\alpha} \cdot N \quad \text{Eq.3}$$

$$\beta\,(h) = 0.846 - 0.015 \ln(h+1) + 0.003139\,(\ln(h+1))^2 \quad \text{Eq.4}$$

where $\phi(h)$ is the total muon flux at depth z (muons cm^{-2} yr^{-1} sr^{-1}), σ_0 is the reference nuclear reaction cross section at muon energy of 1 GeV (millibarn, mb), $\beta(h)$ is the unitless parameterized depth dependence factor (Eq. 4), $\bar{E}(h)$ is the mean muon energy at depth h (GeV), α is a power factor that describes the energy dependence of the cross section (unitless), and N is the number of target nuclei per gram target mineral. The overall production rate of ^{14}C from fast muons provided by Heisinger et al. (2002a) has a high (±50%) uncertainty because of the uncertainty of the reference nuclear reaction cross section σ_0 ($\sigma_0 = 0.0088 \pm 0.0049$ mb). Following Lupker et al. (2015), in this study we used f_{tot} and σ_0 as tuning parameters for the two muogenic production mechanisms in a cosmogenic nuclide production model (Section 3.2) to fit our ^{14}C measurements.

1.3. Gas extraction methods for ice core ^{14}C analysis

Common methods to liberate gas trapped in ice core bubbles include melting (wet extraction; e.g., Sowers et al., 1992; Mitchell et al., 2011) and mechanical destruction of the ice lattice (dry extraction; e.g., Bereiter et al., 2013; Ahn et al., 2009; Zumbrunn et al., 1982). Dry extraction is generally preferable for CO_2 analysis because the presence of liquid water in a wet extraction introduces extraneous CO_2 from the carbonate-acid reaction between the meltwater and impurities in the ice (e.g., Delmas et al., 1980; Raynaud et al., 1982). Multiple studies of $^{14}CO_2$ in ice have used dry extraction methods (e.g., Van De Wal et al., 1994; Smith et al., 2000; Van der Kemp et al., 2000; Van De Wal et al., 2007). However, dry extraction systems (e.g., Lüthi et al., 2008) can potentially introduce biases in CO_2 mole fraction [CO_2] due to incomplete gas extraction (Bereiter et al., 2015). Considering that the *in situ* cosmogenic production of ^{14}C occurs directly in the ice lattice (Lal et al., 1990), it has been argued that dry extraction may also not liberate all of the ^{14}C from the ice (e.g., van Roijen et al., 1994).

Other studies of ^{14}C in ice (e.g., Lal et al., 1990; Jull et al., 1994; Lal et al., 1997, 2001) have used wet extraction methods. These wet-extraction studies involved an addition of acid to drive off all dissolved CO_2 from the meltwater (Lal et al., 1990; Jull et al., 1994; Lal et al., 1997, 2001). The acidification process may have resulted in an additional CO_2 release from impurities in the ice (e.g., carbonate dust). In dust-rich Greenland ice, the presence of liquid water in a wet extraction produced "*in-extractu*" excess CH_4 (Lee et al., 2020). It is thus possible that a wet extraction approach for ^{14}C analysis may also result in additional C release from organics in the ice, which are not ^{14}C-free.

A third method to liberate gases trapped in ice cores is sublimation under vacuum (e.g., Wilson and Donahue, 1989; Wilson and Long, 1997; Wilson and Donahue, 1990; Siegenthaler et al., 2005; Schmitt et al., 2011). Sublimation can occur when the pressure and temperature on the surface of the ice are below the triple point of the water phase change diagram. In addition to being free of problems associated with wet

extraction methods, sublimation guarantees 100% gas extraction efficiency (Schmitt et al., 2011; Bereiter et al., 2013, 2015) which includes any ^{14}C trapped in the ice lattice. Therefore, sublimation is likely an optimal method for $^{14}CO_2$ measurements in ice.

This study presents new ^{14}C measurements in 3 gas species (^{14}CO, $^{14}CO_2$, and $^{14}CH_4$) in ancient (>50 ka BP) ice from the ablation zone of Taylor Glacier, Antarctica to constrain the compound-specific ^{14}C production rates in ice by muons. Ice at this location does not contain a significant amount of ^{14}C inherited from the accumulation site (Petrenko et al., 2016), and the ^{14}C content is due entirely to production by muons during transport within the glacier. We improved on the earlier work by Petrenko et al. (2016) by (1) using a newly developed ice sublimation extraction device for $^{14}CO_2$ measurements (see Section 2.3.2), (2) collecting deeper samples to ~72 m to better characterize the ^{14}C production rate from the fast muon mechanism, and (3) using a more realistic 2D ice-flow model from Buizert et al. (2012) to account for the flow trajectory and exposure history of the samples (see Section 3.1).

2. Field Sampling and Analytical Methods

2.1. Site Description

The blue ice area of Taylor Glacier (Fig. 2) provides access to near-unlimited amounts of well-dated ancient ice (Baggenstos et al., 2017; Bauska et al., 2016; Menking et al., 2019; Schilt et al., 2014; Shackleton et al., 2020). This allows Taylor Glacier ice to be measured for ultra-trace gas species that require a very large amount of ice (Dyonisius et al., 2020; Petrenko et al., 2016, 2017; Buizert et al., 2014). In this study, we used the same site as Petrenko et al. (2016) (77°43.699′S, 161°43.179′), where ice >50 ka in age at the surface has been previously identified.

2.2. Field sampling

Approximately 1000 kg of ice is needed to obtain both the necessary CH_4-derived and CO-derived C mass for ^{14}C analyses. Because of this large sample requirement, and to avoid post-coring *in situ* ^{14}C production at the surface, the melt extraction for $^{14}CH_4$ and ^{14}CO samples was performed on-site using the large volume melter apparatus and technique described in Petrenko et al. (2016). The liberated air was transferred to 34.9 L electropolished stainless steel canisters and shipped to our laboratories for processing and analyses. Similar to other studies using this large volume ice melter (e.g., Dyonisius et al., 2020; Petrenko et al., 2016, 2017), four procedural blanks (two with 'modern' $^{14}CH_4$ standard gas and two with '^{14}C-dead' $^{14}CH_4$ standard gas) were collected in the field. These field procedural blanks allow us to characterize the addition of extraneous ^{14}C to the samples. The standard gases used in the field procedural blanks were passed through a Sofnocat 423 reagent which removes CO (and thus ^{14}CO) but leaves CH_4 (and $^{14}CH_4$) intact.

The sampling scheme for this study is shown in Fig. S1. We used the 9.5-inch diameter Blue Ice Drill (BID) (Kuhl et al., 2014) to collect 7 large-volume samples during the 2015/2016 austral summer field season for ^{14}CO and $^{14}CH_4$ analyses. The "surface" sample was collected from 21 x 1.5m deep shallow cores, each with an average mid-depth of ~ 0.75m. Six additional deep samples with mid-depths of 19.5m, 30m, 40.5m, 51m, 61.5m, and 72m were also collected by combining ice from three ~78m deep boreholes. Each of the deep large-volume samples spanned approximately 10.5m depth. Continuous "sticks" of ice subsamples (3x3 cm, spanning the whole length of the core) were taken from one of the three ice core boreholes ("TGDeep3") for age control (see Supplementary Material Section 3). The continuous sample sticks were measured for CH_4 mole fraction [CH_4] using the continuous flow analysis (CFA) system described in Rhodes et al. (2013) at Oregon State University (OSU).

In addition to the large volume samples, we collected 26 smaller subsamples (~1.5-2 kg) from 13 depth levels and 2 boreholes for $^{14}CO_2$ measurements. Each depth level contained a pair of replicates; however, only 9 out of the 13 replicate pairs were "true" replicates (i.e., collected from the same borehole and cut from the same depth interval, Fig. S1). Collecting same depth-adjacent samples below 50 m depth from a single borehole was challenging because of reduced core quality (i.e., more fractures in the ice), and thus the "replicates" had to be collected from a different borehole. Immediately after removal from the borehole, ice samples become exposed to a more intense cosmic ray bombardment (post-coring *in situ* cosmogenic ^{14}C production). Five artificial "bubble-free-ice" (BFI) samples were manufactured in the field following methods from Mitchell et al. (2011) but upscaled to produce 1.5-2 kg samples. The field-produced BFI samples were shipped together with the collected glacial ice samples to characterize the effects of the post-coring *in situ* cosmogenic $^{14}CO_2$ production in the samples.

2.3. Laboratory analytical methods

2.3.1. Large volume samples for ^{14}CO and $^{14}CH_4$ measurements

The detailed approach for sample processing, measurements and associated procedural corrections for the large volume samples have been previously described in detail (Petrenko et al., 2016). In this section, we only provide a brief overview and highlight the differences between our methods and those of Dyonisius et al. (2020). First, the $\delta^{13}CH_4$ measurements were conducted at the Institute of Arctic and Alpine Research (INSTAAR) following methods described by Miller et al. (2002) (Table S1). The $\delta^{13}CH_4$ measurements were not corrected for gravitational (Sowers et al., 1992) and diffusive isotopic fractionation (Buizert et al., 2013) because these corrections are only necessary to reconstruct the paleoatmospheric $\delta^{13}CH_4$ signal. In this study, the $\delta^{13}CH_4$ values are only used to normalize and calculate the absolute $^{14}CH_4$ abundance (in molecules/g ice).

The large volume samples and field procedural blanks were measured for [CH_4] using a gas chromatograph – multidetector (GC-MD) system (Prinn et al., 2008) (Table S2). Pressure in the sample canisters was measured using a Paroscientific Inc. Digiquartz Series 740 absolute pressure transducer at Scripps Institution of Oceanography (SIO) for total air content (TAC) determination (Table S3). Two of the field procedural blanks were also measured for Kr/N_2, Xe/N_2, and Xe/Kr ratio (Table S4) at Scripps Institution of Oceanography (SIO) following procedures described in Bereiter et al. (2018). The noble gas ratios were used to constrain the degree of gas solubility during the melt extraction. The large volume samples were measured for CO mole fraction [CO] using a Picarro G2401 analyzer (Table S5) and again for pressure at the University of Rochester (UR, Table S4).

The CH_4 in the large volume samples and blanks was combusted to CO_2, cryogenically separated, and flame-sealed in glass ampules using the air processing line at the University of Rochester (Dyonisius et al., 2020). We also processed 3 x 100 μg of CH_4-derived C samples each from the "modern" $^{14}CH_4$ standard gas and "^{14}C-dead" standard gas used for the field procedural blanks. The sample air that remained after CH_4 processing (~10 L STP) was diluted with a gas containing 10.02 ± 0.26 μmol/mol (95% confidence interval, CI) of ^{14}C-depleted CO (^{14}CO = 0.19 ± 0.08 pMC, 95% CI) to increase the CO-derived C mass for the Accelerator Mass Spectrometry (AMS) measurements. The dilutant gas was measured for δ^{13}CO using methods described in Vimont (2017) (δ^{13}CO = -23.36 ± 0.2‰, 95%CI).

The CO- and CH_4-derived CO_2 was graphitized using the Australian Nuclear Science and Technology Organization (ANSTO) "micro" furnaces following Yang and Smith (2017). We used the ^{14}C activity measured on the 100 μg samples as the "true" ^{14}C activity of the standard gases (Table S6). Because of the larger sample size, the effect of extraneous C introduced by graphitization on these 100 μg samples is assumed to be negligible. Using a mass balance approach described in Petrenko et al. (2017), the total extraneous C mass for the $^{14}CH_4$ samples was determined to be 0.63 ± 0.28 μgC, and the corresponding ^{14}C activity for the extraneous C was 16.7 ± 10.2 pMC (95% CI).

In prior studies (e.g., Dyonisius et al., 2020; Petrenko et al., 2017), ^{14}CO measurements from the field procedural blanks were used to characterize the effects of extraneous ^{14}C addition from sample extraction, handling, storage, transport, and processing (including the graphitization step). For this study, the field procedural blanks were still used to characterize the effects from *in situ* production of ^{14}CO in the sample air canisters by cosmic rays during storage and transport. However, to better characterize the effects from the addition of extraneous C during the graphitization process, we used a linear empirical correction from 10 commensurately-sized ^{14}C standards and blanks at ANSTO (see Supplementary Materials, Fig. S2A, Table S7) following Petrenko et al. (2021). This approach has the benefit of bracketing the effects of extraneous C from graphitization at ANSTO with low and high ^{14}C standards, similar to the approach for the $^{14}CH_4$ samples. The ^{14}CO blank for this sample set is 22.45 ± 3.24 molecules ^{14}CO/cc STP (95% CI), which is higher than the ^{14}CO blanks reported in Dyonisius et al. (2020). This is mainly because there was an extra

year between the retrieval and processing of the samples (thus there was more *in situ* ^{14}CO production in sample canisters during storage). $^{14}CH_4$ and ^{14}CO measurements in our samples after all associated corrections, as well as earlier Taylor Glacier results from Petrenko et al. (2016) are shown in Table 1 and Fig. 3.

2.3.2. Sublimation and processing of samples for $^{14}CO_2$ measurements

CO_2 was liberated from ice samples using a newly developed ice sublimation device at the University of Rochester (Hmiel, 2020), roughly following the design of Schmitt et al. (2011). To briefly summarize the procedure, 1.5-2 kg ice samples were loaded into a vacuum glass vessel, the vessel was then evacuated, and the ice was sublimated at vacuum with six infrared emitters (Emitted Energy, USA) for 8-10 hours. We did not sublimate 100% of the samples because as the ice sublimates away, impurities such as dust and organics start to accumulate on the surface. The aggregation of impurities on the sublimation front might enhance unwanted chemical reactions that produce extraneous carbon (Schmitt et al., 2011). Furthermore, towards the end of the extraction, the sublimation became less efficient as less surface area was available to absorb radiation. Approximately 1 kg of ice was sublimated in 8-10 hours. However, the incomplete sublimation does not compromise the 100% extraction efficiency as all the gases trapped in the ice that is sublimated away is still released (Schmitt et al., 2011).

The liberated CO_2 was cryogenically trapped with liquid nitrogen and the air was also cryogenically trapped with 5Å molecular sieve (Sigma Aldrich, USA) under liquid nitrogen. After the sublimation was completed, the trapped CO_2 and air were expanded into separate volume-calibrated manometers where pressure measurements were taken to calculate the [CO_2]. Finally, the isolated CO_2 was cryogenically transferred to and flame-sealed into a Pyrex glass ampule. The CO_2 was graphitized at ANSTO using the "micro" furnaces (Yang and Smith, 2017) and the graphitized samples were measured for ^{14}C activity at the ANTARES AMS facility (Smith et al., 2010). One $^{14}CO_2$ sample (replicate for 30m depth sample) was unfortunately lost during sublimation because the ice fractured under vacuum during the evacuation step.

A ~50-75 g ice subsample was taken from every $^{14}CO_2$ sample and shipped to OSU. The aliquots were measured for [CO_2] following Ahn et al. (2009), and [CH_4] and TAC following Mitchell et al. (2013) (Table S8). Five field-produced bubble-free ice (BFI) samples and 9-laboratory produced BFI samples were also sublimated along with the glacial ice samples. During the sublimation of the BFI samples, a standard gas with known $^{14}CO_2$ activity and [CO_2] was introduced into the bottom of the glass sublimation vessel at 0.15 scc/min flow rate for 8-10 hours. The flow rate was set to mimic the rate of air liberation from glacial ice samples and the processing time also mimicked the amount of time needed to sublimate glacial ice samples. We used a standard gas with "dead" $^{14}CO_2$ activity for 4 laboratory-produced BFI samples and a standard gas with "modern" $^{14}CO_2$ activity for the other 5 laboratory-produced BFI samples. The CO_2 was cryogenically trapped downstream, processed, and measured for ^{14}C activity following the same methods as

the ice samples. In combination with the OSU [CO_2] and TAC measurements, the BFI samples were used to constrain the amount of extraneous carbon and ^{14}C introduced by sample transport, storage, and processing (see Supplementary Materials Section 1, Table S9). Finally, 11 commensurately-sized ^{14}C standards and blanks (14-16 μgC) with known ^{14}C activities (in 0-135 pMC range) were prepared, graphitized and measured at ANSTO concurrently with all the samples (Table S7) to characterize the effects from the addition of extraneous C during the graphitization process.

The detailed corrections for the $^{14}CO_2$ samples are discussed in the Supplementary Materials. We correct for the effects of extraneous C from graphitization and other ANSTO processing using a linear empirical correction from the commensurately-sized ^{14}C standards (Section 1.1 of the Supplementary Materials, Fig. S2B). The effects of extraneous carbon from ice sublimation/CO_2 extraction are calculated from the difference in measured ^{14}C activity of the laboratory-produced BFI samples relative to the measured ^{14}C activity of the standard gases with a mass balance approach (Section 1.2 of the Supplementary Materials, Tables S8 and S9). Finally, the samples were corrected for the effects of post-coring in situ $^{14}CO_2$ production in ice using results from the field-produced BFI samples (Section 1.3 of the Supplementary Materials, Table S10). The $^{14}CO_2$ measurements in our samples after all associated corrections with their error-propagated uncertainties are shown in Table 1 and Fig. 3.

An in-depth discussion about the analytical uncertainty of the $^{14}CO_2$ measurements obtained from the sublimation method (which is important to the interpretation of the data because it is the largest source of uncertainty for total ^{14}C) are provided in Section 1.4 of the Supplementary Materials. In brief, we used the pooled standard deviation of replicate pairs (±7.8 $^{14}CO_2$ molecules/g ice, 2σ) as the uncertainty for all $^{14}CO_2$ measurements except the 2.25 m sample pair (where we used the error-propagated uncertainties instead, Table 1). For the rest of the paper, we refer to the sum of measured ^{14}CO, $^{14}CO_2$, and $^{14}CH_4$ as "total ^{14}C." The $^{14}CH_4/^{14}CO$ ratio, ^{14}CO/total ^{14}C fraction and $^{14}CO_2$/total ^{14}C fraction of the samples are shown in Fig. 4.

2.4. Sample integrity

Several samples were excluded from the data analysis; detailed reasoning for rejecting these samples is discussed in Sections 2 and 3 of the Supplementary Materials. The surface samples (0.75m depth) for all three ^{14}C species (^{14}CO, $^{14}CH_4$, $^{14}CO_2$) are rejected because of ambient air contamination from abundant fractures in the ice sample (due to thermal stresses in near-surface ice) and likely chemical and/or biological alteration of CH_4, CO, and CO_2. The 19.5m and 30m ^{14}CO and $^{14}CH_4$ samples from 2015/2016 season were rejected because of anomalous alterations in TAC, [CO], and [CH_4]. The 30m $^{14}CO_2$ sample was also rejected due to alteration in [CO_2].

3. Estimating the muogenic ^{14}C production rates

3.1. Ice flow model to constrain sample exposure history

We used a 2D ice flow model from Buizert et al. (2012) to generate flow trajectories for the ice parcels corresponding to each sample depth (Fig. 5). The model first computes the 2D steady-state ice-flow velocity field based on the observed surface velocities, ablation rates, and glacier thickness, then generates an ice parcel back-trajectory using 2D linear interpolation of the ice-flow velocity field (Kavanaugh et al., 2009a; Kavanaugh and Cuffey, 2009; Kavanaugh et al., 2009b; Bliss et al., 2011). The largest source of uncertainty for the trajectories are the ablation rates (Buizert et al., 2012), which are based on measurements of 163 poles initially planted in 2002/2003 (Kavanaugh et al., 2009b; Bliss et al., 2011). All survey poles were measured a year later, providing 1-yr average ablation rate estimates (Kavanaugh et al., 2009b) and again in 2006/2007 season. Additionally, 17 poles were remeasured in 2009/2010 and 2010/2011 seasons (Buizert et al., 2012). The 4-yr average ablation rates were 4.7cm yr^{-1} higher than the 1-yr average (Kavanaugh et al., 2009b); following Buizert et al. (2012), the ablation rate uncertainty for each pole was calculated by dividing 4.7cm yr^{-1} with $\sqrt{N}$ where N is the length of the observation period in years (N = 1, 4, 7 or 8). Fig. S3 shows the ablation rates along the glacier and their uncertainties inferred from survey pole data.

The ice flow model used a bedrock profile from Kavanaugh et al. (2009a); however, the bedrock profile only extends to 72 km away from the glacier terminus, a point which we refer to as the glacier head (Fig. 5). This bedrock profile corresponds to 5-6 kyr of ice flow history and approximately one ^{14}C half-life. Beyond the constraints from the bedrock profile, we had to make assumptions about the depth of long-term transport (z_{deep}). Morse et al. (1998) provided a radar-based bedrock profile that includes the Taylor Glacier snow accumulation area (Baggenstos et al., 2018) north of Taylor Dome – approximately 60 km upstream from the glacier head where the Kavanaugh et al. (2009a) bedrock profile ends. Based on the bedrock profile from Morse et al. (1998), at the Taylor Glacier accumulation area, the depth of ~ 80 kyr ice (which corresponds to our 72 m sample) is ~ 575 m. We thus assumed that the depth of long-term transport (z_{deep}) for the 72 m sample under the best-estimate ablation rate scenario (which we define as the reference sample) is 575 m. For other ice parcel trajectories (i), we scaled the depth of long-term transport (z_{deep}) following

$$z_{deep}(i) = 575 - (z_{ref} - z_{head}(i)) \quad \text{Eq.5}$$

where z_{ref} represents the depth of the 72 m reference sample in the model at the glacier head under the best-estimate flowline (z_{ref} is 699 m) and z_{head} represents the depth of the ice parcel of interest at the glacier head. We assumed that the difference in depth between the reference sample and the sample of interest (i) at the glacier head and during long-term transport within the glacier is the same.

3.2. ^{14}C production in sample ice parcel

We used the model for *in situ* cosmogenic nuclide production by muons from Balco et al. (2008), with all relevant parameters adjusted for ice (Fig.1). This model in turn uses the Heisinger et al. (2002a, 2002b)

parameterizations described above and additional altitude scaling of the muon fluxes. We then used a forward model that numerically integrates the total ^{14}C in the ice sample along its flow path in Taylor Glacier. For initial condition, we assumed that at the depth of long-term transport (z_{deep}), the ^{14}C concentration in the ice parcel is at steady state:

$$\frac{dC}{dt}(\text{at } z_{deep}) = 0 = P_{neg}(z_{deep}) + P_{fast}(z_{deep}) - C_0\lambda \quad \text{Eq.6}$$

The steady state assumption means that at z_{deep}, the rate of radioactive decay ($C_0\lambda$) is balanced by production from negative muon capture (P_{neg}) and fast muon reaction (P_{fast}). For each ice parcel, we calculated the steady-state, initial ^{14}C concentration (C_0) from Eq.6, then used the following differential equation

$$\frac{dC}{dt} = P_{neg}(z(t)) + P_{fast}(z(t)) - C\lambda \quad \text{Eq.7}$$

to numerically integrate the ^{14}C concentration of the ice parcel along the flow trajectory. To avoid interference from spallogenic (neutron-produced) ^{14}C, we only considered samples deeper than 6.85m depth.

We sampled the parameter space in a "grid search" approach to obtain the best-estimate values for muogenic ^{14}C production parameters σ_0 and f_{tot}. Using the best-estimate flow trajectory, we calculated the expected ^{14}C in the samples corresponding to all combinations of σ_0 and f_{tot}, with each of the parameters ranging between 0-100% of the values from Heisinger et al. (2002a, 2002b). To save computational time, we first conducted the grid search at a coarse resolution of 10% increments (Fig. S4A). The goodness of the fit (χ^2) for each simulation was calculated following:

$$\chi^2 = \sum \frac{(C_{obs}(z) - C_{exp}(z))^2}{C_{exp}(z)} \quad \text{Eq.8}$$

where $C_{obs}(z)$ is the measured total ^{14}C and $C_{exp}(z)$ is the total ^{14}C ($^{14}CO_2$ + ^{14}CO + $^{14}CH_4$; Fig. 3D) calculated by the forward model at sample depth z. To find more precise best-estimate σ_0 and f_{tot}, we conducted the grid-search again at a higher resolution of 0.2% increments from Heisinger et al. (2002a, 2002b) values near the χ^2 minimum, between 0 to 0.0352 millibarn for σ_0 and 0 to 0.01 for f_{tot} (Fig. S4B).

To estimate the uncertainties in σ_0 and f_{tot}, we used a Monte Carlo sampling of model parameters. We assumed that the ablation rate uncertainties (Fig. S3) represent 2σ normally distributed uncertainties. We then perturbed the ablation rates within their uncertainties and generated a pool of 10,000 possible flow trajectories for each sample depth. However, in 69 out of 10,000 flow scenarios, the ice parcel back-trajectories hit the bedrock and became unphysical afterwards. These unphysical trajectories were removed from the pool of possible ice flow trajectories. Next, we started with the best-estimate σ_0 and f_{tot} and assumed a normally distributed and large 200% (1σ) error for each parameter (Fig. S5A) as prior distribution for the Monte Carlo method. We removed σ_0 and f_{tot} values that are below zero from the prior distribution because they are unphysical and conducted 100,000 Monte Carlo simulations using the forward ^{14}C production model. For each Monte Carlo simulation, we randomly picked one of the previously generated possible ice flow trajectories and a random pair of σ_0 and f_{tot} from the generated prior distributions (Fig. S5A). We then

calculated the expected ^{14}C concentrations for each sample depth using the forward model and compared the model-data fit. We accept all pairs of σ_0 and f_{tot} values that produce model-calculated total ^{14}C within the 95% CI (7.8 ^{14}C atoms g^{-1} ice) and 67% CI (3.9 ^{14}C atoms g^{-1} ice) analytical uncertainty of the best-fit, model-calculated total ^{14}C (black line, Fig. 6). The ranges of accepted σ_0 and f_{tot} pairs are shown in Fig. 7A as contours. The discussion about the selection of acceptance criteria for estimating σ_0 and f_{tot} uncertainties is provided in Section 1.4 of the Supplementary Material.

3.3 ^{14}CO production model in sample ice parcel

The in-situ cosmogenic ^{14}CO production rates in ice are of specific interest as discussed in Section 1.1. To characterize the ^{14}CO production rates, we introduced additional scaling factors f_{neg} and f_{fast} for negative muon and fast muon mechanisms, respectively as tuned model parameters. The differential equation of Eq.7 is modified into

$$\frac{d(^{14}CO)}{dt} = f_{neg}P_{neg}(z(t)) + f_{fast}P_{fast}(z(t)) - (^{14}CO)\lambda \qquad \text{Eq.9}$$

We note that P_{neg} and P_{fast} in Eq.9 are the total ^{14}C production rates calculated from the Balco et al. (2008) model. The scaling factors f_{neg} and f_{fast} each encompasses 2 terms, one that adjusts the total ^{14}C production rates and another that accounts for the ^{14}CO fraction of total ^{14}C. The determination of best-estimate f_{neg} and f_{fast} and their uncertainties were similar to the approach for σ_0 and f_{tot} described above. χ^2 "grid-search" was conducted with all combinations of f_{neg} and f_{fast} values ranging from 0 to 0.2 at 0.001 resolution (Fig. S4C). Similar to the total ^{14}C data, we used the average analytical uncertainty of the ^{14}CO sample set as the acceptance criteria for the Monte Carlo simulations to estimate the uncertainties of f_{neg} and f_{fast}. We accepted all sets of f_{neg} and f_{fast} from the 100,000 Monte Carlo simulations that yielded model-predicted ^{14}CO within 1.2 ^{14}CO molecules g^{-1} ice (95% CI uncertainty) and 0.6 ^{14}CO molecules g^{-1} ice (68% CI uncertainty) from the best-fit model (Fig. 8). Fig. 7B shows (as contours) the accepted sets of f_{neg} and f_{fast} values.

3.3. Comparison with Scharffenbergbotnen ablation site

Van der Kemp et al. (2002) measured $^{14}CO_2$ and ^{14}CO in ice from the Scharffenbergbotnen ice ablation site, Antarctica. Using a 1D ablation model, we examined how the estimates of muogenic ^{14}C production rates from Taylor Glacier compare to the Scharffenbergbotnen data. We assumed that the measured $^{14}CO_2$ + ^{14}CO from Scharffenbergbotnen are comparable to our measurements of total ^{14}C in Taylor Glacier ice (since our data show that less than 0.3% of total ^{14}C from muon production forms $^{14}CH_4$, Section 4.1). We then used the ^{14}C concentration from the deepest Scharffenbergbotnen sample (45 m) as the initial condition. In the 1D ablation model, the Scharffenbergbotnen ice parcel moves upward at a rate (dz/dt) equal to the ablation rate from stake measurements (Eq.10, a = 16 ± 4 cm yr^{-1}).

$$\frac{dz}{dt} = -a \qquad \text{Eq.10}$$

$$\frac{dC}{dt} = P'n(z(t)) + P'_{neg}(z(t)) + P'_{fast}(z(t)) - C\lambda \qquad \text{Eq.11}$$

The expected ^{14}C concentration in the ice is given by the differential equation (Eq.11) where P'_n is the ^{14}C spallogenic production rate from Young et al. (2014), P'_{neg} and P'_{fast} are the muogenic production rates inferred from Taylor Glacier data scaled to the elevation of Scharffenbergbotnen (1173m above sea level) using altitude scaling factors from Balco et al. (2008). We also repeated this calculation for ^{14}CO only, to compare the muogenic ^{14}CO production rates with the ^{14}CO data from Scharffenbergbotnen.

4. Results and Discussions

4.1. Measured ^{14}C values and partitioning of $^{14}CO_2$, ^{14}CO and $^{14}CH_4$

Table 1 and Fig.3a-c show the depth profiles of ^{14}CO, $^{14}CH_4$ and $^{14}CO_2$ after all corrections. For the $^{14}CO_2$ measurements, comparison with prior results that used a wet extraction approach (Fig. S6) confirms the caveats discussed by Petrenko et al. (2016) that their $^{14}CO_2$ measurements were uncertain and represent the upper bound. The $^{14}CH_4/^{14}CO$ ratios from the new samples (0.0074 ± 0.0004, 95% CI, n=4, from all samples below 19.5m) appear to be constant within uncertainties (Fig. 4A), in agreement with earlier results (0.0076 ± 0.0004, 95% CI, n=4) from Petrenko et al. (2016). This confirms that the two muon reactions produce ^{14}C in a constant $^{14}CH_4/^{14}CO$ ratio. The ^{14}CO and $^{14}CO_2$ fractions of total ^{14}C are also relatively constant at depth (Fig. 4B) – suggesting that the two muon reactions produce all three ^{14}C species in constant ratios.

For samples deeper than 6.85m, on average 33.7% (±11.4%, 95% CI) of the produced cosmogenic ^{14}C becomes ^{14}CO and 66.1% (±11.5%, 95% CI) of the produced cosmogenic ^{14}C becomes $^{14}CO_2$ (Fig. 4B). The uncertainties of ^{14}CO and $^{14}CO_2$ fractions on the deepest samples (72m depth) are relatively large because of the small $^{14}CO_2$ signal (11.8 to 13.6 $^{14}CO_2$ molecules/g ice) relative to the uncertainty of our measurements (±7.8 $^{14}CO_2$ molecules/g ice, 95% CI). The $^{14}CO_2$ fraction in samples that are deeper than 6.85m (0.66 ± 0.12, 95% CI) is also in agreement with prior reported $^{14}CO_2$ fraction of 0.69 from the Scharffenbergbotnen ablation site (Van der Kemp et al., 2002). Finally, the shallow samples (<6m ice equivalent) show higher $^{14}CH_4/^{14}CO$ ratios (Fig. 4A) and $^{14}CO_2$/total ^{14}C ratios. This may indicate that neutron-induced spallation produces higher amounts of $^{14}CH_4$ and $^{14}CO_2$ relative to ^{14}CO (Petrenko et al., 2016) or that CO (and ^{14}CO) is not well-preserved in near-surface ice of Taylor Glacier due to potential microbial activities.

At depths where production from muons dominates (>6 m ice equivalent), less than 0.3% of the produced cosmogenic ^{14}C in ice forms $^{14}CH_4$ (Table 1, Fig. 4). Although the $^{14}CH_4$ measurement from the 10 m depth sample is not available (Petrenko et al., 2016), we still include the 10 m data point in the total ^{14}C dataset used to infer σ_0 and f_{tot} values and their uncertainties. The contribution from $^{14}CH_4$ (which would have been

on the order of ~ 0.2 $^{14}CH_4$ molecules/g ice, Fig. 3B) is insignificant compared to the uncertainty in total ^{14}C. We account for the lack of $^{14}CH_4$ measurement at this depth by scaling the total ^{14}C of the 10 m sample by a factor of 1.003 ± 0.003 (95% CI, Table 1).

4.2. Inferred muogenic ^{14}C production rates in ice as compared to estimates from studies in quartz

Assuming that the majority of *in situ* cosmogenic ^{14}C in ice forms $^{14}CO_2$, ^{14}CO, and $^{14}CH_4$, the muogenic ^{14}C production parameters from Heisinger et al. (2002a, 2002b) (f_{tot} for negative muon capture and σ_0 for fast muon reaction) are well outside the confidence intervals of our measurements (Table 2, Figs. 6A and 7A). Using the larger uncertainty for $^{14}CO_2$ measurements obtained from step-by-step error propagation (Section 1.4 of Supplementary Materials, Fig. S7) does not change this conclusion. Our results indicate that the overall probability of the negative muon capture reaction (f_{tot}) and reference cross-section for fast muon mechanism (σ_0) for production of ^{14}C from ^{16}O in ice (hence the muogenic *in situ* ^{14}C production rates) given by Heisinger et al. (2002a, 2002b) are too high by factors of 5.7 (3.6-13.9, 95% CI) and 3.7 (2.0-11.9, 95% CI) respectively.

One possible explanation for the disagreement between our results and those of Heisinger et al. (2002a, 2002b) is that our ^{14}C measurements (mostly either ^{14}CO or $^{14}CO_2$, as $^{14}CH_4$ only constitutes <0.3% of total ^{14}C) might be incorrect. However, in the following we thoroughly explore this possibility and argue that it is unlikely. Our ^{14}CO measurements used a well-established analytical technique (e.g., Dyonisius et al., 2020; Hmiel et al., 2020; Petrenko et al., 2013, 2017, 2021). With regards to ^{14}CO measurements in air, this analytical technique (Petrenko et al., 2021) yields comparable results to independent, atmospheric ^{14}CO measurements from other research groups (e.g., Manning et al., 2005; Mak and Southon, 1998). We also have no reason to believe that there is a systematic loss of ^{14}CO during ice melting process. The ice melting (wet extraction) ensures that all ^{14}C and CO is liberated. CO is not very soluble in water (the dissolved CO fraction at equilibrium in our system is on the order of 1%) and we used the measured δXe/Kr (Table S4) to correct for the solubility effects for both [CO] and [CH_4]. The on-site field extraction, within hours of sample retrieval ensures that there is minimal post-coring gas loss. Finally, ice core and firn air ^{14}CO measurements at Greenland Summit are consistent within uncertainties with muogenic ^{14}CO production rates inferred from Taylor Glacier (Hmiel et al., 2020; Hmiel, 2020).

The sublimation technique used for our $^{14}CO_2$ measurements also ensures 100% extraction efficiency of gases (Schmitt et al., 2011). We tested the system performance by sublimating BFI (bubble-free-ice) samples while adding standard gases with known $^{14}CO_2$ activities. As mentioned in Section 2.3.2, we used two standard gases with known $^{14}CO_2$ activities, one with "modern" $^{14}CO_2$ activity and the other with "dead" $^{14}CO_2$ activity when sublimating BFI samples. There is no significant alteration in the CO_2 mole fraction and $^{14}CO_2$ activity of both standard gases (Table S8) or in CO_2 mole fraction of the ice samples (Table S9), which suggests that the processes of sublimating ice and flowing gas through the system components do not result in loss of $^{14}CO_2$. Finally, we can also rule out the possibility of post-coring $^{14}CO_2$ loss. In a separate

measurement campaign (Hmiel 2020), we brought the sublimation system to Summit, Greenland and sublimated the ice samples on-site (within days from the time when the ice core was drilled). We compared the $^{14}CO_2$ from the on-site, field sublimation with the $^{14}CO_2$ from depth-adjacent replicates sublimated at the University of Rochester laboratory and found that they are indistinguishable within uncertainty.

Another strong indication that our measurements are robust is the good agreement with independent results from Van der Kemp et al. (2002). Van der Kemp et al. (2002) measured $^{14}CO_2$ and ^{14}CO in ice from Scharffenbergbotnen ice ablation site using a dry extraction technique. The total measured ^{14}C values were significantly lower than the expected values based on the stake-measured ablation rates and muogenic production rates based on laboratory irradiations of quartz targets (Heisinger et al., 2000a, 2002b). Van der Kemp et al. (2002) hypothesized that the low extraction efficiency of dry mechanical extraction (which can result in an incomplete release of the *in situ* produced ^{14}C from the ice grains) might be responsible for this discrepancy. As mentioned above, we used a sublimation method for our $^{14}CO_2$ measurements and a melt extraction method for our ^{14}CO measurements; both methods guarantee that all *in situ* cosmogenic ^{14}C in the ice lattice is released. Fig.8 shows that the Scharffenbergbotnen data are consistent with the expected total ^{14}C and ^{14}CO from Taylor Glacier-derived production rates.

As mentioned above, we also find good agreement in the ratio of ^{14}C compounds ($^{14}CO_2$ fraction = 0.66 ± 0.12 in this study, 0.69 in Van der Kemp et al., 2002). This strongly suggests that our extraction methods and analytical techniques were not systematically losing ^{14}CO or $^{14}CO_2$ (which would then bias the $^{14}CO_2$ and ^{14}CO fraction). It is theoretically possible that both our measurements and Van der Kemp et al. (2002) are wrong. However, to produce the same ratio of ^{14}C compounds, it would require all 3 analytical systems from these studies to be systematically wrong in the same direction and by the same magnitude – which is highly unlikely. The good agreement between Taylor Glacier and Scharffenbergbotnen data suggests that dry mechanical extraction is a valid technique for extracting $^{14}CO_2$ and ^{14}CO from bubbly, non-clathrated ice cores. One possible explanation is that after production, *in situ* $^{14}CO_2$ and ^{14}CO quickly migrates from the ice matrix to the air bubbles. This result is consistent with previous observations that the retention of in situ cosmogenic ^{14}C in firn grains is very low (Petrenko et al., 2013; Van der Kemp et al., 2000; Wilson and Donahue, 1992).

One way to reconcile our and Van der Kemp et al. (2002) measurements with the Heisinger et al. (2002a, 2002b) production rates would be to have much higher (factor of 3 or greater) long term (hundreds to thousands of years) ablation rates at Taylor Glacier and Scharffenbergbotnen compared to recent ablation stakes measurements. The ablation rate over the last 100 years is especially important with regards to *in situ* ^{14}C production rate from negative muon capture (Fig. S9). Ablation rate at blue ice areas is controlled by climate via a combination of temperature, insolation, and wind (mainly katabatic) (e.g., Bintanja, 1999). To get much higher long-term ablation rates at both Taylor Glacier and Scharffenbergbotnen (which are on opposite sides of Antarctica), we would need either the temperatures to have dropped sharply in the last

couple of decades, the winds to have slowed dramatically, or for insolation to have sharply decreased. However, the two deep ice cores nearest to Taylor Glacier, Taylor Dome (Steig et al., 2000) and RICE (Roosevelt Island Climate Evaluation) (Bertler et al., 2018) do not show large climate changes in the region over the last 1,000 years. The glaciological survey of Taylor Glacier also indicated that the glacier is approximately at steady-state given the stake-measured ablation rates (Kavanaugh et al. 2009a, 2009b). The 30-year record of weather observations over the McMurdo Dry Valleys area show that the recent climate in this region is stable (Obryk et al., 2020). Finally, a 14-year-long observation study (Sinisalo et al., 2003) over the Scharffenbergbotnen blue ice area also showed no significant recent change in the ablation rates. We thus argue that a large decrease in ablation rates in recent years as compared to the long-term average (over the last hundreds to thousands of years) does not seem to be a realistic explanation.

For direct comparison with other studies, we used the scaling factors from Lifton et al. (2014) to calculate the corresponding sea level high latitude (SLHL) total ^{14}C and ^{14}CO-specific production rates in ice (Tables 2 and 3). Our estimates of the ^{14}CO-specific production rates agree with those of Petrenko et al. (2016) within errors (Table 3). Compared with the results from Petrenko et al. (2016), we also calculated a slightly smaller uncertainty on the ^{14}CO-specific production rate by negative muon capture (Table 3). We also converted the Lupker et al. (2015) estimates of f_{tot} in quartz into f_{tot} for ice (Table 2), using the chemical compound factors (f_C) for quartz and ice from Heisinger et al. (2002b). With regards to negative muon capture, the Lupker et al. (2015) estimate of f_{tot} is in close agreement with Heisinger et al. (2002b) (Table 2). However, the high f_{tot} in Lupker et al. (2015) as compared to our result was offset by their best σ_0 estimate of zero (lower than our result). For a direct comparison with results from Lupker et al. (2015), we fit our data while forcing σ_0 (and hence ^{14}C production from fast muons) to be zero (Fig. 6b) and cannot find a scenario with reasonable model-data agreement.

Because of the relatively large uncertainty of the $^{14}CO_2$ measurements, the total ^{14}C data still allow σ_0 to be close to zero given a sufficiently large f_{tot} (Fig. 7A). However, our ^{14}CO data (which have much lower relative uncertainties and use a more established measurement technique) unambiguously show that σ_0 and ^{14}C production from fast muon cannot be zero (Fig. 8, Fig. 7B). As discussed in Lupker et al. (2015), the ^{14}C data from the 15.5 m Leymon-High quartzite core might not cover the depth range where production from fast muons dominates. In contrast, when integrated over the whole flow history, production from fast muons represents the dominant source of ^{14}C in our deeper samples. The very high-end estimate of our reference nuclear reaction cross section σ_0 (for ^{14}C production from fast muons) is still within the large uncertainty of σ_0 from both Heisinger et al. (2002a) and Lupker et al. (2015) (Table 2). However, our estimated total probability of negative muon capture (f_{tot}) (and hence the ^{14}C production rate from negative muon) is well outside the confidence intervals of f_{tot} reported by both Heisinger et al. (2002b) and Lupker et al. (2015) (Table 2).

One caveat to our estimated *in situ* muogenic ^{14}C production rates in ice (and that of Van der Kemp et al., 2002) is that the total ^{14}C from the gas species we measured (^{14}CO, $^{14}CO_2$, and $^{14}CH_4$) might not account for all muogenic *in situ* ^{14}C. Although $^{14}CO_2$ and ^{14}CO likely constitute the large majority (Lal et al., 1997, 2000), a small amount of *in situ* ^{14}C can also form ^{14}C-bearing organic materials. Measurements of ^{14}C in organic carbon from alpine ice for the purpose of radiocarbon dating have shown elevated ^{14}C values attributed to *in situ* cosmogenic production (Fang et al., 2021; Hoffmann, 2016). A laboratory irradiation experiment of glacier ice with an artificial neutron flux showed that 11-25% of produced ^{14}C forms organic compounds (Hoffmann, 2016). Earlier work involving irradiation of ice samples to produce ^{14}C (e.g., Roessler et al., 1984) also found that organics accounted for a minor fraction of total ^{14}C. However, we are not aware of any existing studies that specifically investigated production of ^{14}C-bearing organic materials in ice from muons. Measuring ^{14}C in organic compounds is unfortunately beyond the scope of this study, as it requires an entirely different analytical setup.

Another possible explanation for the disagreement is that the 2D ice flow model (and thus the time dependent, exposure history of the ice parcels) might be inaccurate. In the following, we conducted sensitivity analyses to combine both uncertainties by using the +2.4σ maximum ablation rate scenario (which corresponds to the deepest physically possible ice trajectory, Fig. S8) and scaling our total ^{14}C upward by 25% to account for the *in situ*-produced ^{14}C in organics (red dots, Fig. 6D). First, we kept f_{tot} as a constant (f_{tot} = 0.021, which is the minimum f_{tot} from the reported uncertainty in Heisinger et al. 2002b) and tuned σ_0 to fit the measurements (dashed red line, Fig. 6D) under high ablation rate scenario. We find that the best-fit σ_0 (and *in situ* ^{14}C production from fast muon) is zero. The modeled total ^{14}C under this scenario underestimates the total ^{14}C at lower depths where production from fast muon dominates (>20 m depth) and overestimates the total ^{14}C at depths where production from negative muon capture dominates (<20 m depth). This means that even under these extreme scenarios, the ^{14}C production rate from negative muon capture has to be lower than the lower-bound estimate of Heisinger et al. (2002b) and some production from fast muons is needed to compensate the lower production rate from negative muon capture to improve the fit. We then repeated our "grid-search" approach (Section 3.2) to find the best-fit f_{tot} and σ_0 that correspond to the 25% higher total ^{14}C and maximum ablation rate scenario (solid red line, Fig. 6D). The best-fit f_{tot} is 0.0055 which is 22% of Heisinger et al. 2002b value) and the best-fit σ_0 is 0.0040 mb (which is 46% of Heisinger et al. 2002a value). We note that these values are within uncertainties of original our best-fit f_{tot} and σ_0 (Table 2). We conclude that additional uncertainties from the ice flow history and ^{14}C contribution from organics likely cannot reconcile the difference between the negative muon capture ^{14}C production rate inferred by our data and that of Heisinger et al. (2002b).

Finally, it may also be possible that the overall probability of ^{14}C production from negative muon capture on ^{16}O in ice is lower than predicted by Heisinger et al. (2002) based on their laboratory irradiations of quartz targets, if for example either the f_C or f_D factors (Eq. 2) were incorrectly estimated. In their experimental

determination of the ^{14}C production rate by fast muons, Heisinger et al. (2002a) used a single muon energy of 190 GeV ($\sigma(E)$). The reference nuclear reaction cross section at 1 GeV (σ_0) was then scaled using the following equation

$$\sigma(E) = \sigma_0 \bar{E}^{\alpha} \quad \text{Eq.12}$$

where α is a power factor that describes the energy dependence of the cross section (unitless). However, the mean muon energy ($\bar{E}$) of 190 GeV used by Heisinger et al. (2002a), as well as the muon flux intensity were much higher than those expected in the first few hundred meters of ice in natural settings (for the top 200m of Taylor Glacier ice, $\bar{E}$ = 32 GeV Fig. S10). It is possible that the power factor α might be incorrect or that the experimental results of Heisinger et al (2002a, 200b) are not directly transferrable to natural settings.

5. Conclusions

This study presents $^{14}CO_2$ measurements in ablating ice obtained via a new ice sublimation technique, combined with ^{14}CO and $^{14}CH_4$ measurements obtained from a well-established large-volume melt-extraction method to estimate the species-specific and total *in situ* muogenic ^{14}C production rates in ice. Under the assumption that the majority of *in situ* ^{14}C in ice exists as ^{14}CO, $^{14}CO_2$, and $^{14}CH_4$, our results indicate that commonly used literature values for rates of *in situ* production of ^{14}C by muons in ice are overestimated by a factor of 5.7 (3.6-13.9, 95% CI) and 3.7 (2.0-11.9, 95% CI) for negative muon capture and fast muon interactions, respectively. Comparison between the data presented in this study and prior ice core data from Scharffenbergbotnen (Van der Kemp et al., 2002) strengthens this conclusion. This comparison also suggests that a dry extraction technique appears to release essentially all *in situ* ^{14}C in bubbly (non-clathrated) ice.

The constraints on muogenic ^{14}C production rates in ice and the partitioning between the in-situ produced ^{14}C-bearing gas species provided by this study will allow for future measurements of ^{14}C-containing gases in other ice cores to be used for several applications, including using $^{14}CO_2$ measurements for absolute dating of the bubbles in ice cores (Andree et al., 1984; Van De Wal et al., 1994) and using ^{14}CO measurements to either constrain the oxidative capacity of the atmosphere (Brenninkmeijer et al., 1992; Petrenko et al., 2021) or reconstruct the past cosmic ray flux (BenZvi et al., 2019).

At present, there does not appear to be a way to reconcile our results and independent data from Scharffenbergbotnen in ice (Van der Kemp et al., 2002) with muogenic ^{14}C production rates in quartz (Heisinger et al., 2002a, 2002b; Lupker et al., 2015). This is a problem that needs further investigation, and we recommend that future studies address this via laboratory muon irradiation experiments involving both ice and quartz targets, as well as studies that include quantification of the organic fraction of muogenic ^{14}C in ice.

Data availability

Data from this work will be available through the USAP Data Center (https://www.usap-dc.org/data).

Author Contributions

VVP, EJB and JPS designed the study. MND and VVP conducted field logistical preparations. MND, VVP, PN, AMS, JAM, SAS, HR, BB, EJB and JRM conducted the field sampling, on-site sample cutting and processing. MND, VVP, AMS and PN extracted the large air samples using the on-site large volume melter. MND extracted the CH_4 and CO from large air samples. BH, VVP, MND, and PFP developed and tested the sublimation system with input from JS. MND extracted the CO_2 using the newly built sublimation system with assistance from BH and PFP. QH and BY graphitized the ^{14}C samples. AMS conducted the ^{14}C measurements. CA and JAM conducted the CH_4 CFA measurements under supervision of EJB. CA developed the age-scale under supervision of EJB. SEM and IV made the $\delta^{13}C$-CH_4 stable isotopes measurements. JPS made the Xe/Kr, Kr/N_2 and Xe/N_2 measurements. RB made the $\delta^{15}N_2$, $\delta^{18}O_{atm}$, $^{40}Ar/^{36}Ar$, O_2/N_2 and Ar/N_2 measurements. CH made the [CH_4] and halogenated trace gas measurements under supervision of RFW. MK made the discrete [CH_4] mole fraction and total air content measurements. IV made the $\delta^{13}CO$ measurement for the CO dilution gas. CB developed the ice flow model. MND developed the ^{14}C production model with input from CB and VVP. MND, BH, and VVP analysed the results and wrote the manuscript with input from all authors.

Competing interests

We declare no competing interests

Acknowledgements

We thank Mike Jayred of the U.S. Ice Drilling Program (IDP) for ice drilling, camp manager Kathy Schroeder for assistance in the field, and United States Antarctic Program (USAP) for logistical support. We thank Emily Mesiti for her assistance in the Rochester ice core lab during the sublimation extraction campaign. This work was supported by US NSF awards PLR-1245659 (Petrenko), PLR-1245821 (Brook), PLR-1246148 (Severinghaus) and Packard Fellowship for Science and Engineering (Petrenko).

References

Ahn, J., Brook, E. J., and Howell, K.: A high-precision method for measurement of paleoatmospheric CO2 in small polar ice samples, *J. Glaciol*, **55**, 499–506, 2009.

Andree, M., Moor, E., Beer, J., Oeschger, H., Stauffer, B., Bonani, G., Hofmann, H. J., Morenzoni, E., Nessi, M., and Suter, M.: ^{14}C dating of polar ice, *Nucl. Instrum. Meth. B*, **5**, 385–388, 1984.

Baggenstos, D., Bauska, T. K., Severinghaus, J. P., Lee, J. E., Schaefer, H., Buizert, C., Brook, E. J., Shackleton, S., and Petrenko, V. V.: Atmospheric gas records from Taylor Glacier, Antarctica, reveal ancient ice with ages spanning the entire last glacial cycle, *Clim. Past.*, **13**, 943, 2017.

Baggenstos D., Severinghaus J. P., Mulvaney R., McConnell J. R., Sigl M., Maselli O., Petit J.-R., Grente B. and Steig E. J.: A horizontal ice core from Taylor Glacier, its implications for Antarctic climate history, and an improved Taylor Dome ice core time scale, *Paleoceanogr Paleoclimatol*, **33**(7), 778–794, 2018.

Balbas, A. M. and Farley, K. A.: Constraining in situ cosmogenic nuclide paleo-production rates using sequential lava flows during a paleomagnetic field strength low, *Chem. Geol.*, **532**, 119355, https://doi.org/10.1016/j.chemgeo.2019.119355, 2020.

Balco, G.: Production rate calculations for cosmic-ray-muon-produced ^{10}Be and ^{26}Al benchmarked against geological calibration data, *Quat. Geochronol.*, **39**, 150–173, 2017.

Balco, G.: Glacier change and paleoclimate applications of cosmogenic-nuclide exposure dating, *Annu. Rev. Earth. Pl. Sc.*, **48**, 21–48, 2020.

Balco, G., Stone, J. O., Lifton, N. A., and Dunai, T. J.: A complete and easily accessible means of calculating surface exposure ages or erosion rates from ^{10}Be and ^{26}Al measurements, *Quat. Geochronol.*, **3**, 174–195, 2008.

Bauska, T. K., Baggenstos, D., Brook, E. J., Mix, A. C., Marcott, S. A., Petrenko, V. V., Schaefer, H., Severinghaus, J. P., and Lee, J. E.: Carbon isotopes characterize rapid changes in atmospheric carbon dioxide during the last deglaciation, *PNAS*, **113**, 3465–3470, 2016.

Bereiter, B., Stocker, T. F., and Fischer, H.: A centrifugal ice microtome for measurements of atmospheric CO_2 on air trapped in polar ice cores, *Atmos. Meas. Tech.*, **6**, 251–262, 2013.

Bereiter, B., Eggleston, S., Schmitt, J., Nehrbass-Ahles, C., Stocker, T. F., Fischer, H., Kipfstuhl, S., and Chappellaz, J.: Revision of the EPICA Dome C CO_2 record from 800 to 600 kyr before present, *Geophys. Res. Lett.*, **42**(2), 541-549, 2015.

Bereiter, B., Kawamura, K., and Severinghaus, J. P.: New Methods for Measuring Atmospheric Heavy Noble Gas Isotope and Elemental Ratios in Ice Core Samples, *Rapid. Commin. Mass. Sp* **32**, 801–814, 2018.

Bertler, N. A. N., Conway, H., Dahl-Jensen, D., Emanuelsson, D. B., Winstrup, M., Vallelonga, P. T., Lee, J. E., Brook, E. J., Severinghaus, J. P., Fudge, T. J., Keller, E. D., Baisden, W. T., Hindmarsh, R. C. A., Neff, P. D., Blunier, T., Edwards, R., Mayewski, P. A., Kipfstuhl, S., Buizert, C., Canessa, S., Dadic, R., Kjær, H. A., Kurbatov, A., Zhang, D., Waddington, E. D., Baccolo, G., Beers, T., Brightley, H. J., Carter, L., Clemens-Sewall, D., Ciobanu, V. G., Delmonte, B., Eling, L., Ellis, A., Ganesh, S., Golledge, N. R., Haines, S., Handley, M., Hawley, R. L., Hogan, C. M., Johnson, K. M., Korotkikh, E., Lowry, D. P., Mandeno, D., McKay, R. M., Menking, J. A., Naish, T. R., Noerling, C., Ollive, A., Orsi, A., Proemse, B. C., Pyne, A. R., Pyne, R. L., Renwick, J., Scherer, R. P., Semper, S., Simonsen, M., Sneed, S. B., Steig, E. J., Tuohy, A., Venugopal, A. U., Valero-Delgado, F., Venkatesh, J., Wang, F., Wang, S., Winski, D. A., Winton, V. H. L., Whiteford, A., Xiao, C., Yang, J., and Zhang, X.: The Ross Sea Dipole – temperature, snow accumulation and sea ice variability in the Ross Sea region, Antarctica, over the past 2700 years, *Clim. Past.*, **14**, 193–214, 2018.

Bliss, A. K., Cuffey, K. M., and Kavanaugh, J. L.: Sublimation and surface energy budget of Taylor Glacier, Antarctica, *J. Glaciol*, **57**, 684–696, 2011.

Brenninkmeijer, C. A. M., Manning, M. R., Lowe, D. C., Wallace, G., Sparks, R. J., and Volz-Thomas, A.: Interhemispheric asymmetry in OH abundance inferred from measurements of atmospheric 14CO, *Nature*, **356**, 50–52 , 1992.

Buizert, C.: ICE CORE METHODS | Studies of Firn Air, in: Encyclopedia of Quaternary Science (Second Edition), edited by: Mock, S. A. E. J., Elsevier, Amsterdam, 361–372, 2013.

Buizert, C., Petrenko, V. V., Kavanaugh, J. L., Cuffey, K. M., Lifton, N. A., Brook, E. J., and Severinghaus, J. P.: In situ cosmogenic radiocarbon production and 2-D ice flow line modeling for an Antarctic blue ice area, *J. Geophys. Res.*, **117**. F2, 2012.

Buizert, C., Sowers, T., and Blunier, T.: Assessment of diffusive isotopic fractionation in polar firn, and application to ice core trace gas records, , *Earth. Planet. Sc. Lett.*, **361**, 110–119 , 2013.

Buizert, C., Baggenstos, D., Jiang, W., Purtschert, R., Petrenko, V. V., Lu, Z.-T., Müller, P., Kuhl, T., Lee, J., Severinghaus, J. P., and Brook, E. J.: Radiometric 81Kr dating identifies 120,000-year-old ice at Taylor Glacier, Antarctica, *PNAS*, **111**, 6876–6881, 2014.

Delmas, R. J., Ascencio, J.-M., and Legrand, M.: Polar ice evidence that atmospheric CO_2 20,000 yr BP was 50% of present, *Nature*, **284**, 155–157, 1980.

Dyonisius, M., Petrenko, V. V., Smith, A. M., Hua, Q., Yang, B., Schmitt, J., Beck, J., Seth, B., Bock, M., Hmiel, B., Vimont, I., Menking, J. A., Shackleton, S., Baggenstos, D., Bauska, T. K., Rhodes, R. H., Sperlich, P., Beaudette, Ross, Harth, C. M., Kalk, M. L., Brook, E. J., Fischer, H., Severinghaus, J., and Weiss, R. F.: Old carbon reservoirs were not significant in the deglacial methane budget, *Science*, **357**, 907–910, 2020.

von Egidy, T. and Hartmann, F. J.: Average muonic Coulomb capture probabilities for 65 elements, *Phys. Rev. A*, **26**, 2355–2360, 1982.

Fang, L., Jenk, T. M., Singer, T., Hou, S., and Schwikowski, M.: Radiocarbon dating of alpine ice cores with the dissolved organic carbon (DOC) fraction, *Cryosphere*, **15**, 1537–1550, 2021.

Fenton, C. R., Niedermann, S., Dunai, T., and Binnie, S. A.: The SPICE project: Production rates of cosmogenic 21Ne, 10Be, and 14C in quartz from the 72 ka SP basalt flow, *Quat. Geochronol.*, **54**, 101019, 2019.

Gosse, J. C. and Phillips, F. M.: Terrestrial in situ cosmogenic nuclides: theory and application, *Quaternary Sci. Rev.*, **20**, 1475–1560, 2001.

Heisinger, B., Lal, D., Jull, A. J. T., Kubik, P., Ivy-Ochs, S., Neumaier, S., Knie, K., Lazarev, V., and Nolte, E.: Production of selected cosmogenic radionuclides by muons: 1. Fast muons, *Earth. Planet. Sc. Lett.*, **200**, 345–355, 2002a.

Heisinger, B., Lal, D., Jull, A. J. T., Kubik, P., Ivy-Ochs, S., Knie, K., and Nolte, E.: Production of selected cosmogenic radionuclides by muons: 2. Capture of negative muons, *Earth. Planet. Sc. Lett.*, **200**, 357–369, 2002b.

Herron, M. M. and Langway, C. C.: Firn densification: an empirical model, *J. Glaciol*, **25**, 373–385, 1980.

Hippe, K.: Constraining processes of landscape change with combined in situ cosmogenic ^{14}C-^{10}Be analysis, *Quaternary Sci. Rev*, **173**, 1–19, 2017.

Hmiel, B.: A Study of In Situ Cosmogenic ^{14}C and Paleoatmospheric $^{14}CH_4$ From Accumulating Ice at Summit, Greenland, PhD Thesis, University of Rochester, 2020.

Hmiel, B., Petrenko, V. V., Dyonisius, M., Buizert, C., Smith, A. M., Place, P. F., Harth, C. M., Beaudette, R., Hua, Q., Yang, B., Vimont, I., Michel, S. E., Severinghaus, J. P., Etheridge, D. M., Bromley, T. M., Schmitt, J., Fain, X., Weiss, R. F., and Dlugokencky, E. J.: Preindustrial $^{14}CH_4$ indicates that anthropogenic fossil CH_4 emissions are underestimated, *Nature*, **578**(7795), 409-412, 2020.

Hoffmann, M.: Micro radiocarbon dating of the particulate organic carbon fraction in Alpine glacier ice: method refinement, critical evaluation and dating applications, PhD Dissertation, University of Heidelberg, 2016.

Hogg, A. G., Heaton, T. J., Hua, Q., Palmer, J. G., Turney, C. S., Southon, J., Bayliss, A., Blackwell, P. G., Boswijk, G., and Ramsey, C. B.: SHCal20 Southern Hemisphere calibration, 0–55,000 years cal BP, *Radiocarbon*, **62**, 759–778, 2020.

Jull, A. T., Lal, D., Donahue, D. J., Mayewski, P., Lorius, C., Raynaud, D., and Petit, J. R.: Measurements of cosmic-ray-produced ^{14}C in firn and ice from Antarctica, *Nucl. Instrum. Meth. B*, **92**, 326–330, 1994.

Kavanaugh, J. L. and Cuffey, K. M.: Dynamics and mass balance of Taylor Glacier, Antarctica: 2. Force balance and longitudinal coupling, *J. Geophys. Res.*, **114**, F04011, 2009.

Kavanaugh, J. L., Cuffey, K. M., Morse, D. L., Conway, H., and Rignot, E.: Dynamics and mass balance of Taylor Glacier, Antarctica: 1. Geometry and surface velocities, *J. Geophys. Res*., **114**, F04010, 2009a.

Kavanaugh, J. L., Cuffey, K. M., Morse, D. L., Bliss, A. K., and Aciego, S. M.: Dynamics and mass balance of Taylor Glacier, Antarctica: 3. State of mass balance, *J. Geophys. Res.*, **114**, F04012, 2009b.

Kuhl, T. W., Johnson, J. A., Shturmakov, A. J., Goetz, J. J., Gibson, C. J., and Lebar, D. A.: A new large-diameter ice-core drill: the Blue Ice Drill, *Ann. Glaciol.*, **55**, 1–6, 2014.

Kutschera, W.: The Half-Life of ^{14}C—Why Is It So Long?, *Radiocarbon*, **61**, 1135–1142, 2019.

Lal, D. and Jull, A. J. T.: On determining ice accumulation rates in the past 40,000 years using in situ cosmogenic ^{14}C, *Geophys. Res. Lett.*, **17**, 1303–1306, 1990.

Lal, D., Jull, A. J. T., Donahue, D. J., Burtner, D., and Nishiizumi, K.: Polar ice ablation rates measured using in situ cosmogenic ^{14}C, *Nature*, **346**, 350–352, 1990.

Lal, D., Jull, A. T., Burr, G. S., and Donahue, D. J.: Measurements of in situ ^{14}C concentrations in Greenland Ice Sheet Project 2 ice covering a 17-kyr time span: Implications to ice flow dynamics, *J. Geophys. Res-Oceans*, **102**, 26505–26510, 1997.

Lal, D., Jull, A. J. T., Burr, G. S., and Donahue, D. J.: On the characteristics of cosmogenic in situ 14C in some GISP2 Holocene and late glacial ice samples, *Nucl. Instrum. Meth. B*, **172**, 623–631, 2000.

Lal, D., Jull, A. J. T., Donahue, D. J., Burr, G. S., Deck, B., Jouzel, J., and Steig, E.: Record of cosmogenic in situ produced 14C in Vostok and Taylor Dome ice samples: Implications for strong role of wind ventilation processes, *J. Geophys. Res.*, **106**, 31933–31941, 2001.

Lee, J. E., Edwards, J. S., Schmitt, J., Fischer, H., Bock, M., and Brook, E. J.: Excess methane in Greenland ice cores associated with high dust concentrations, *Geochim. Cosmochim. Ac.*, **270**, 409–430, 2020.

Lifton, N., Sato, T., and Dunai, T. J.: Scaling in situ cosmogenic nuclide production rates using analytical approximations to atmospheric cosmic-ray fluxes, *Earth. Planet. Sc. Lett*, **386**, 149–160, 2014.

Lifton, N., Caffee, M., Finkel, R., Marrero, S., Nishiizumi, K., Phillips, F. M., Goehring, B., Gosse, J., Stone, J., Schaefer, J., Theriault, B., Jull, A. J. T., and Fifield, K.: In situ cosmogenic nuclide production rate calibration for the CRONUS-Earth project from Lake Bonneville, Utah, shoreline features, *Quat. Geochronol*., **26**, 56–69, 2015.

Lupker, M., Hippe, K., Wacker, L., Kober, F., Maden, C., Braucher, R., Bourlès, D., Romani, J. R. V., and Wieler, R.: Depth-dependence of the production rate of in situ 14C in quartz from the Leymon High core, Spain, *Quat. Geochronol*., **28**, 80–87, 2015.

Lüthi, D., Le Floch, M., Bereiter, B., Blunier, T., Barnola, J.-M., Siegenthaler, U., Raynaud, D., Jouzel, J., Fischer, H., Kawamura, K., and Stocker, T. F.: High-resolution carbon dioxide concentration record 650,000–800,000 years before present, *Nature*, 453, 379, 2008.

Mak, J. E. and Southon, J. R.: Assessment of tropical OH seasonality using atmospheric ^{14}CO measurements from Barbados, *Geophys. Res. Lett.*, **25**, 2801–2804, 1998.

Manning, M. R., Lowe, D. C., Moss, R. C., Bodeker, G. E., and Allan, W.: Short-term variations in the oxidizing power of the atmosphere, *Nature*, **436**, 1001, 2005.

Menking, J. A., Brook, E. J., Shackleton, S. A., Severinghaus, J. P., Dyonisius, M. N., Petrenko, V., McConnell, J. R., Rhodes, R. H., Bauska, T. K., and Baggenstos, D.: Spatial pattern of accumulation at Taylor Dome during Marine Isotope Stage 4: stratigraphic constraints from Taylor Glacier, *Clim. Past.*, **15**, 1537–1556, 2019.

Miller, J. B., Mack, K. A., Dissly, R., White, J. W., Dlugokencky, E. J., and Tans, P. P.: Development of analytical methods and measurements of 13C/12C in atmospheric CH4 from the NOAA Climate Monitoring and Diagnostics Laboratory Global Air Sampling Network, *J. Geophys. Res-Atmos*, **107**, 2002.

Mitchell, L., Brook, E., Lee, J. E., Buizert, C., and Sowers, T.: Constraints on the Late Holocene Anthropogenic Contribution to the Atmospheric Methane Budget, *Science*, **342**, 964–966, 2013.

Mitchell, L. E., Brook Edward J., Sowers Todd, McConnell J. R., and Taylor Kendrick: Multidecadal variability of atmospheric methane, 1000–1800 C.E., *J. Geophys. Res-Biogeo*, **116**, 2011.

Morse D. L., Waddington E. D., and Steig E. J.: Ice Age storm trajectories inferred from radar stratigraphy at Taylor Dome, Antarctica, *Geophys. Res. Lett.*, **25**, 3383–3386, 1998.

Obryk, M. K., Doran, P. T., Fountain, A. G., Myers, M., and McKay, C. P.: Climate From the McMurdo Dry Valleys, Antarctica, 1986–2017: Surface Air Temperature Trends and Redefined Summer Season, *J.Geophys.Res-Atmos.* **125**, 2020.

Pendleton, S., Miller, G., Lifton, N., and Young, N.: Cryosphere response resolves conflicting evidence for the timing of peak Holocene warmth on Baffin Island, Arctic Canada, *Quaternary Sci. Rev*, **216**, 107–115, 2019.

Petrenko, V. V., Smith, A. M., Brook, E. J., Lowe, D., Riedel, K., Brailsford, G., Hua, Q., Schaefer, H., Reeh, N., Weiss, R. F., Etheridge, D., and Severinghaus, J. P.: $^{14}CH_4$ Measurements in Greenland Ice: Investigating Last Glacial Termination CH4 Sources, *Science*, **324**, 506–508, 2009.

Petrenko, V. V., Severinghaus, J. P., Smith, A. M., Riedel, K., Baggenstos, D., Harth, C., Orsi, A., Hua, Q., Franz, P., Takeshita, Y., Brailsford, G. W., Weiss, R. F., Buizert, C., Dickson, A., and Schaefer, H.: High-precision ^{14}C measurements demonstrate production of in situ cosmogenic $^{14}CH_4$ and rapid loss of in situ cosmogenic ^{14}CO in shallow Greenland firn, *Earth. Planet. Sc. Lett.*, **365**, 190–197, 2013.

Petrenko, V. V., Severinghaus, J. P., Schaefer, H., Smith, A. M., Kuhl, T., Baggenstos, D., Hua, Q., Brook, E. J., Rose, P., Kulin, R., Bauska, T., Harth, C., Buizert, C., Orsi, A., Emanuele, G., Lee, J. E., Brailsford, G., Keeling, R., and Weiss, R. F.: Measurements of ^{14}C in ancient ice from Taylor Glacier, Antarctica constrain in situ cosmogenic $^{14}CH_4$ and ^{14}CO production rates, *Geochim. Cosmochim. Ac.*, **177**, 62–77, 2016.

Petrenko, V. V., Smith, A. M., Schaefer, H., Riedel, K., Brook, E., Baggenstos, D., Harth, C., Hua, Q., Buizert, C., Schilt, A., Fain, X., Mitchell, L., Bauska, T., Orsi, A., Weiss, R. F., and Severinghaus, J. P.: Minimal geological methane emissions during the Younger Dryas–Preboreal abrupt warming event, *Nature*, **548**, 443–446, 2017.

Petrenko, V. V., Smith, A. M., Crosier, E. M., Kazemi, R., Place, P., Colton, A., Yang, B., Hua, Q., and Murray, L. T.: An improved method for atmospheric ^{14}CO measurements, *Atmos. Meas. Tech*, **14**, 2055–2063, 2021.

Prinn, R. G., Weiss, R. F., Krummel, P. B., O'Doherty, S., Fraser, P., Muhle, J., Reimann, S., Vollmer, M., Simmonds, P. G., and Malone, M.: The ALE/GAGE/AGAGE Network, Massachusetts Institute of Technology, Cambridge, MA (USA);, 2008.

Raynaud, D., Delmas, R., Ascencio, J. M., and Legrand, M.: Gas Extraction From Polar Ice Cores: A Critical Issue For Studying The Evolution of Atmospheric CO2 and Ice-Sheet Surface Elevation, *Ann. Glaciol.*, **3**, 265–268, 1982.

Reimer, P. J., Austin, W. E., Bard, E., Bayliss, A., Blackwell, P. G., Ramsey, C. B., Butzin, M., Cheng, H., Edwards, R. L., and Friedrich, M.: The IntCal20 northern hemisphere radiocarbon age calibration curve (0–55 cal kBP), *Radiocarbon*, **62**, 725–757, 2020.

Rhodes, R. H., Faïn, X., Stowasser, C., Blunier, T., Chappellaz, J., McConnell, J. R., Romanini, D., Mitchell, L. E., and Brook, E. J.: Continuous methane measurements from a late Holocene Greenland ice core: Atmospheric and in-situ signals, *Earth. Planet. Sc. Lett.*, **368**, 9–19, 2013.

Roessler, K., H-J. Jung, and B. Nebeling.: Hot atoms in cosmic chemistry, *Advances in Space Research* **4.12**, 83-95, 1984

van Roijen, J. J., Bintanja, R., Van der Borg, K., van den Broeke, M. R., de Jong, A. F. M., and Oerlemans, J.: Dry extraction of 14CO2 and 14CO from Antarctic ice, Nuclear Instruments and Methods in Physics Research Section B: Beam Interactions with Materials and Atoms, *Nucl. Instrum. Meth. B*, **92**, 331–334, 1994.

Schilt, A., Brook, E. J., Bauska, T. K., Baggenstos, D., Fischer, H., Joos, F., Petrenko, V. V., Schaefer, H., Schmitt, J., Severinghaus, J. P., Spahni, R., and Stocker, T. F.: Isotopic constraints on marine and terrestrial N2O emissions during the last deglaciation, *Nature*, **516**, 234–237, 2014.

Schmitt, J., Schneider, R., and Fischer, H.: A sublimation technique for high-precision measurements of δ13CO2 and mixing ratios of CO2 and N2O from air trapped in ice cores, *Atmos. Meas. Tech.*, **4**, 1445–1461, 2011.

Shackleton, S., Baggenstos, D., Menking, J. A., Dyonisius, M. N., Bereiter, B., Bauska, T. K., Rhodes, R. H., Brook, E. J., Petrenko, V. V., McConnell, J. R., Kellerhals, T., Häberli, M., Schmitt, J., Fischer, H., and Severinghaus, J. P.: Global ocean heat content in the Last Interglacial, *Nat. Geosci.*, **13**, 77–81, 2020.

Shackleton, S., Menking, J. A., Brook, E., Buizert, C., Dyonisius, M. N., Petrenko, V. V., Baggenstos, D., and Severinghaus, J. P.: Evolution of mean ocean temperature in Marine Isotope Stages 5-4, *Clim. Past.*, 1–21, 2021.

Siegenthaler, U., Stocker, T. F., Monnin, E., Lüthi, D., Schwander, J., Stauffer, B., Raynaud, D., Barnola, J.-M., Fischer, H., and Masson-Delmotte, V.: Stable carbon cycle–climate relationship during the late Pleistocene, *Science*, 310, 1313–1317, 2005.

Sinisalo, A., Moore, J. C., Wal, R. S. W. V. D., Bintanja, R., and Jonsson, S.: A 14 year mass-balance record of a blue-ice area in Antarctica, *Ann. Glaciol.*, **37**, 213–218, 2003.

Skov, D. S., Egholm, D. L., Jansen, J. D., Sandiford, M., and Knudsen, M. F.: Detecting landscape transience with in situ cosmogenic ^{14}C and ^{10}Be, *Quat. Geochronol.*, **54**, 101008, 2019.

Smith, A. M., Levchenko, V. A., Etheridge, D. M., Lowe, D. C., Hua, Q., Trudinger, C. M., Zoppi, U., and Elcheikh, A.: In search of in-situ radiocarbon in Law Dome ice and firn, *Nucl. Instrum. Meth. B*, **172**, 610–622, 2000.

Smith, A. M., Hua, Q., Williams, A., Levchenko, V., and Yang, B.: Developments in micro-sample ^{14}C AMS at the ANTARES AMS facility, *Nucl. Instrum. Meth. B*, **268**, 919–923, 2010.

Sowers, T., Bender, M., Raynaud, D., and Korotkevich, Y. S.: $\delta^{15}N$ of N2 in air trapped in polar ice: A tracer of gas transport in the firn and a possible constraint on ice age-gas age differences, *J. Geophys. Res.*, **97**, 15683–15697, 1992.

Spector, P., Stone, J., and Goehring, B.: Thickness of the divide and flank of the West Antarctic Ice Sheet through the last deglaciation, *Cryosphere*, **13**, 3061–3075, 2019.

Steig, E. J., Morse, D. L., Waddington, E. D., Stuiver, M., Grootes, P. M., Mayewski, P. A., Twickler, M. S., and Whitlow, S. I.: Wisconsinan and Holocene Climate History from an Ice Core at Taylor Dome, Western Ross Embayment, Antarctica, *Geogr. Ann. A.*, **82**, 213–235, 2000.

van De Wal, R. S. W., Van Roijen, J. J., Raynaud, D., Van der Borg, K., De Jong, A. F. M., Oerlemans, J., Lipenkov, V., and Huybrechts, P.: From $^{14}C/^{12}C$ measurements towards radiocarbon dating of ice, *Tellus. B.*, **46**, 94–102, 1994.

van De Wal, R. S. W., Meijer, H. a. J., De Rooij, M., and Van der Veen, C.: Radiocarbon analyses along the EDML ice core in Antarctica, *Tellus. B*, **59**, 157–165, 2007.

Van der Kemp, W. J. M., Alderliesten, C., Van der Borg, K., Holmlund, P., de Jong, A. F. M., Karlöf, L., Lamers, R. A. N., Oerlemans, J., Thomassen, M., and Van de Wal, R. S. W.: Very little in situ produced radiocarbon retained in accumulating Antarctic ice, *Nucl. Instrum. Meth. B*, **172**, 632–636, 2000.

Van der Kemp, W. J. M., Alderliesten, C., Van der Borg, K., De Jong, A. F. M., Lamers, R. a. N., Oerlemans, J., Thomassen, M., and Van De Wal, R. S. W.: In situ produced ^{14}C by cosmic ray muons in ablating Antarctic ice, *Tellus. B*, **54**, 186–192, 2002.

Vimont, I.: Carbon Monoxide Stable Isotopes: Extraction Technique Development and Urban Atmospheric Analysis, PhD Thesis, University of Colorado Boulder, 2017.

Wilson, A. T. and Donahue, D. J.: The recovery and dating of carbon dioxide in polar ice cores, *Radiocarbon*, **31**, 579–584, 1989.

Wilson, A. T. and Donahue, D. J.: AMS carbon-14 dating of ice: progress and future prospects, *Nucl. Instrum. Meth. B*, **52**, 473–476, 1990.

Wilson, A. T. and Long, A.: New approaches to CO_2 analysis in polar ice cores, *J. Geophys. Res-Oceans*, **102**, 26601–26606, 1997.

Yang, B. and Smith, A. M.: Conventionally Heated Microfurnace for the Graphitization of Microgram-Sized Carbon Samples, *Radiocarbon*, **59**, 859–873, 2017.

Zumbrunn, R., Neftel, A., and Oeschger, H.: CO_2 measurements on 1-cm^3 ice samples with an IR laserspectrometer (IRLS) combined with a new dry extraction device, *Earth. Planet. Sc. Lett.*, **60**, 318–324, 1982.

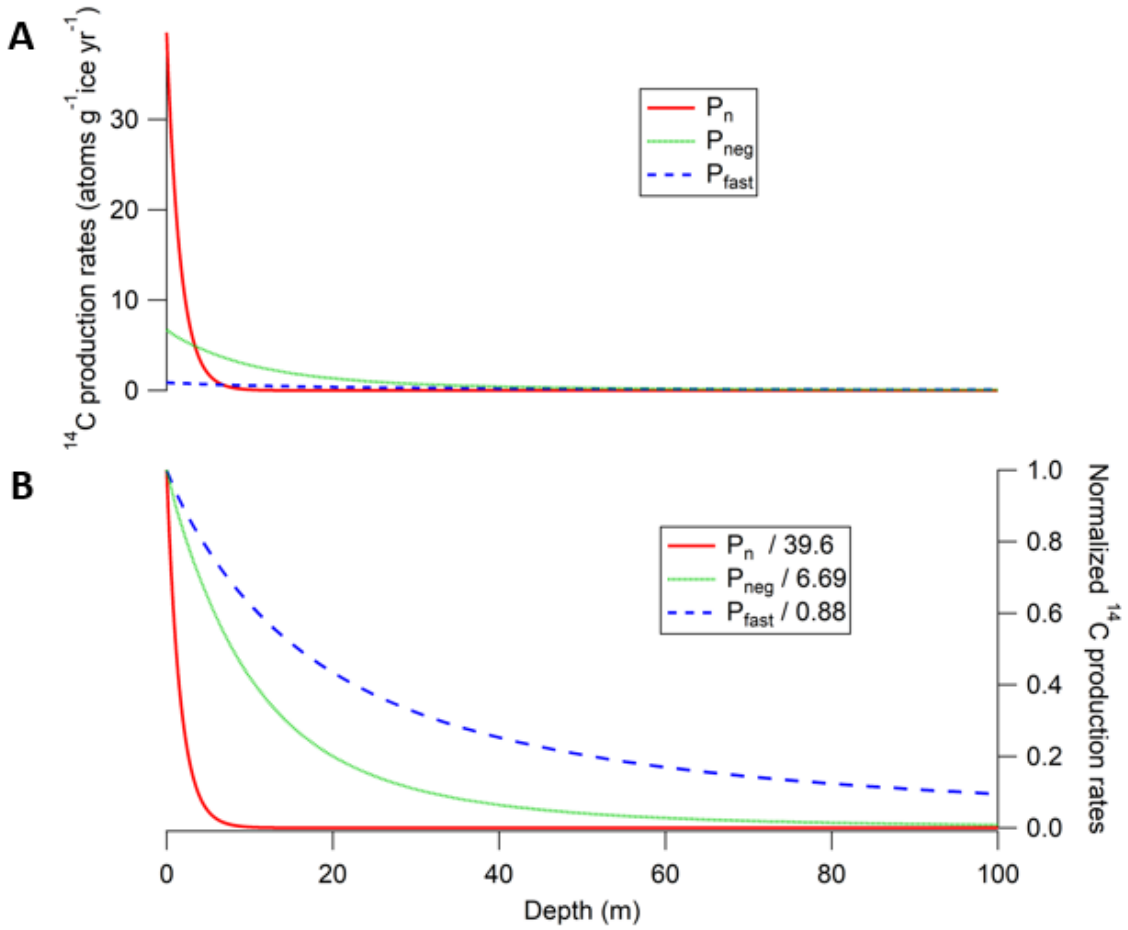

915 **Fig. 1. (A) In-situ cosmogenic ^{14}C production rates scaled for Taylor Glacier study site (77°44′S, 162°10′E, 526m elevation) from the three nuclear mechanisms: neutron-induced spallation (P_n), negative muon capture (P_{neg}), and fast muon interactions (P_{fast}). (B) Depth profiles of the three production mechanisms normalized to their respective surface production rates (the respective surface production rates are shown in the legend).** For ^{14}C production from neutron spallation, we used the surface
920 production rate estimate from Young et al. (2014) with scaling from Lifton et al. (2014). For the two muon mechanisms (negative and fast muons), we used the production rate model from Balco et al. (2008), which follows parametrizations by Heisinger et al. (2002a, 2002b).

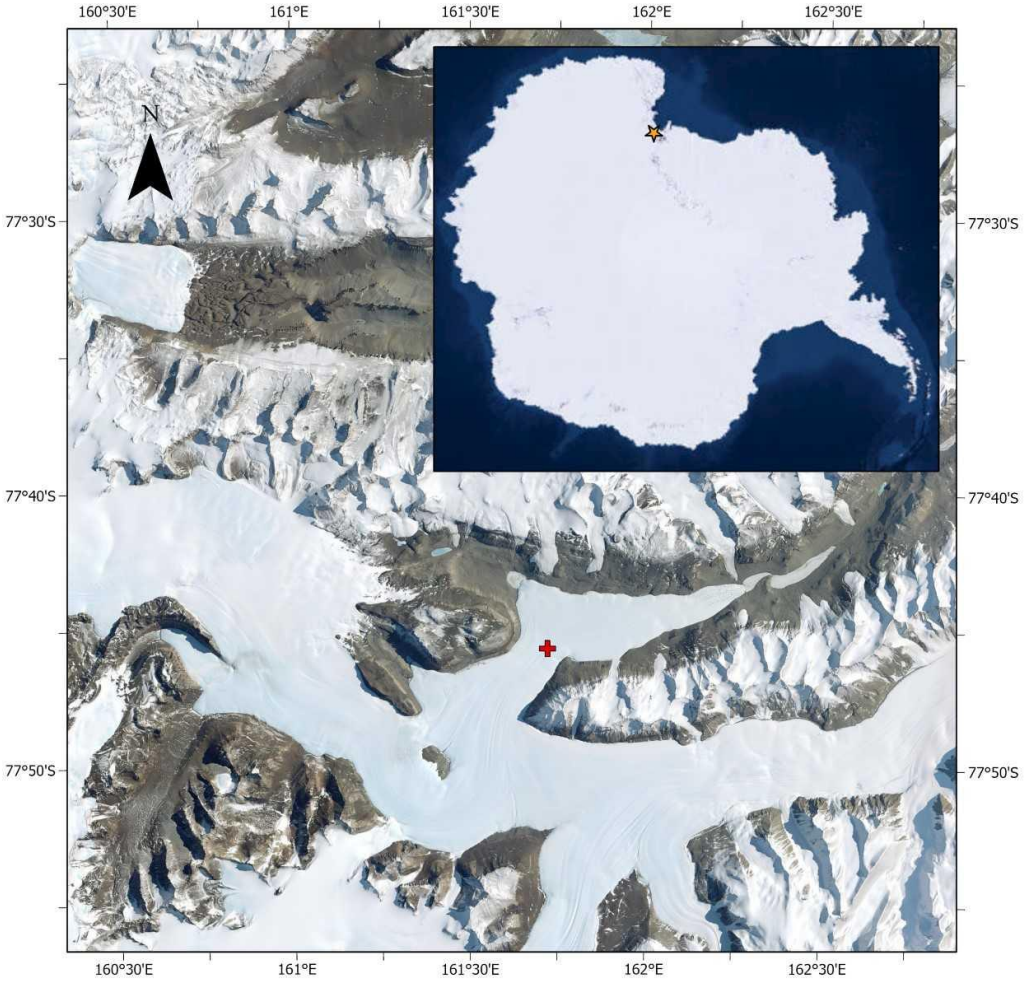

Fig. 2. Map of the Taylor Glacier study site. The sampling location is marked by a red (+) sign on the map. The orange star sign on the inset map shows the location of Taylor Glacier relative to the Antarctic continent. Map made using ArcGIS Pro with Imagery layers from ESRI and EarthStar Geographics.

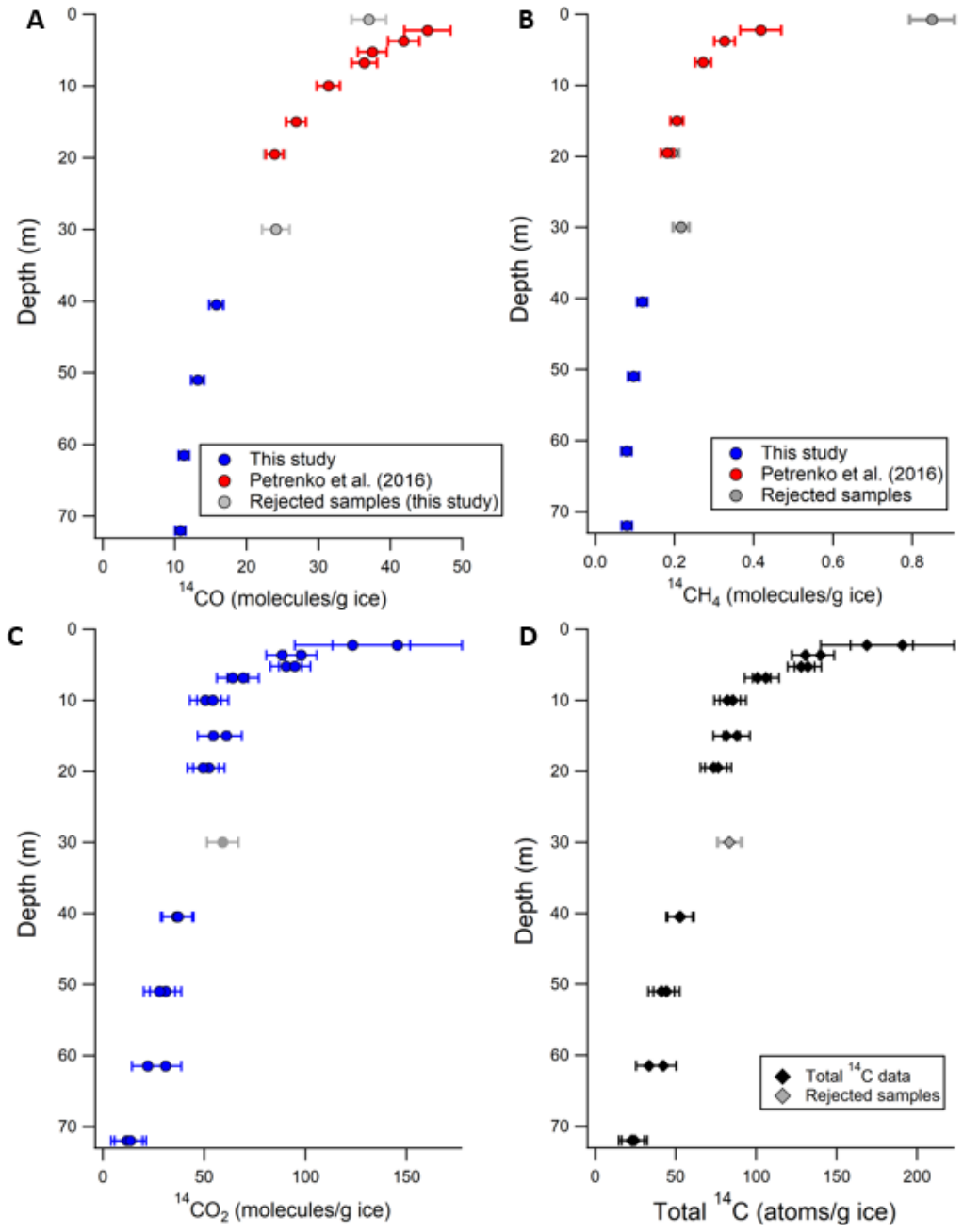

Fig. 3. (A). Measured ^{14}CO molecules/g ice after all corrections. (B) Measured ^{14}CH$_4$ molecules/g ice after all corrections. (C) Measured ^{14}CO$_2$ molecules/g ice after all corrections. (D) Total measured ^{14}C atoms/g ice. This represents the sum of ^{14}CO, ^{14}CH$_4$, and sublimation-based ^{14}CO$_2$ measurements. All error bars shown in this figure are 95% CI.

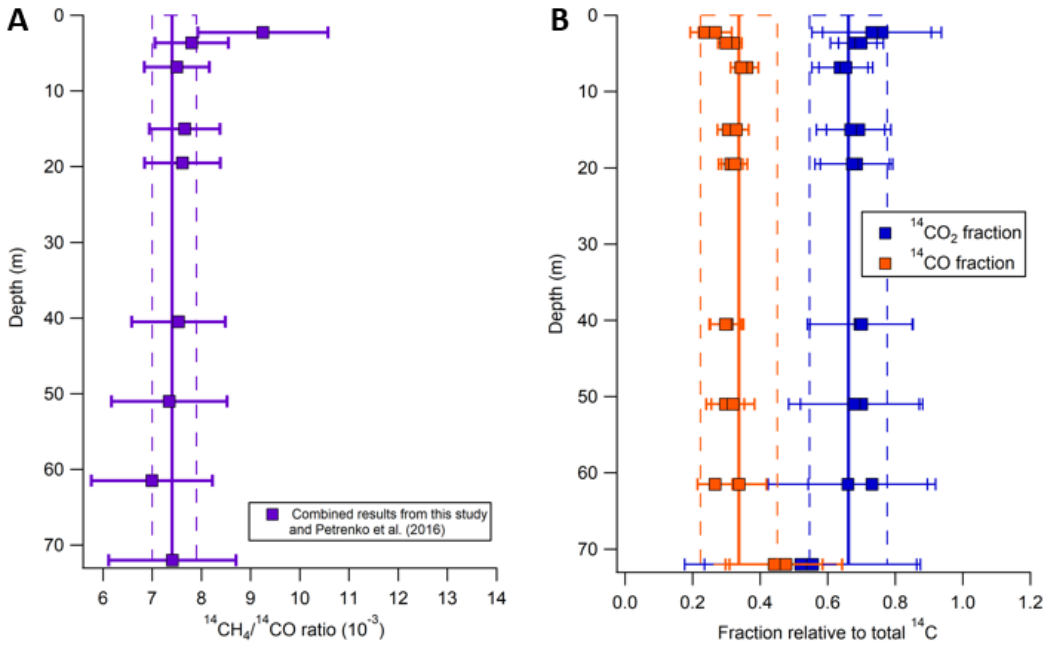

Fig. 4. (A) $^{14}CH_4/^{14}CO$ ratio. (B) ^{14}CO/total ^{14}C fraction and $^{14}CO_2$/total ^{14}C fraction. The solid lines represent the mean and the dashed lines represent 2 standard deviations of the $^{14}CH_4/^{14}CO$ ratio, $^{14}CO_2$ and ^{14}CO fractions for samples deeper than 6.85 m where production by muons dominates. The ratios for rejected samples (Section 4.1, Supplementary Materials Section 2) are not shown. All error bars shown in this figure are 95% CI.

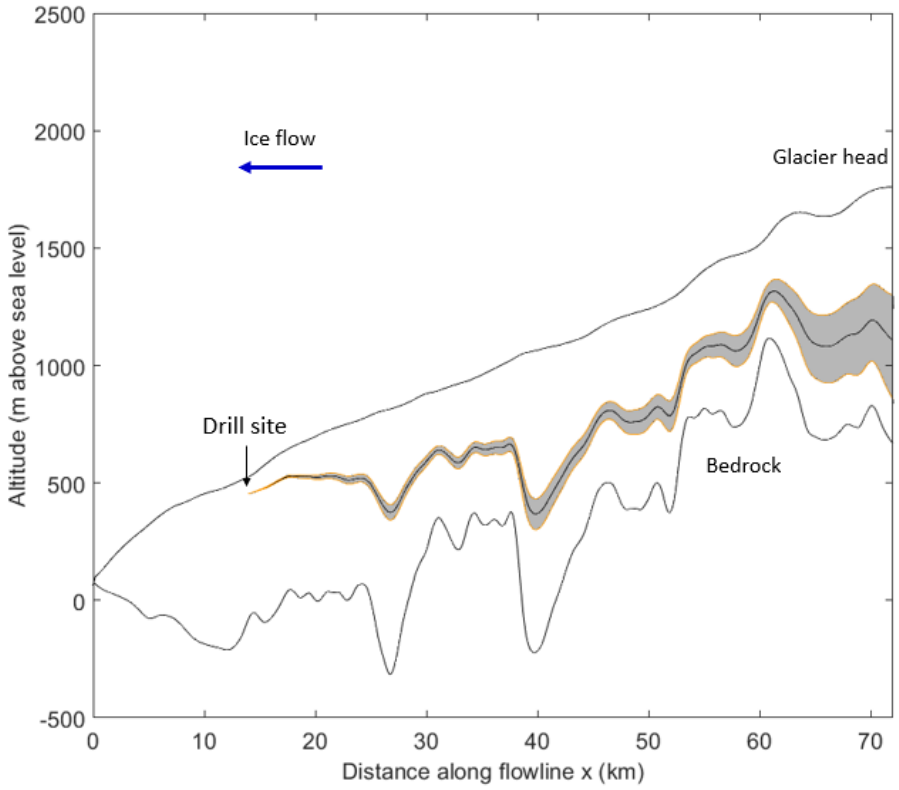

940

Fig. 5. Example of ice parcel back-trajectory and associated uncertainties. For the Monte-Carlo estimate of uncertainties (Section 5.4.2), for each given sample depth (72 m in this figure), 10,000 back trajectories are generated. Each back trajectory corresponds to a different ablation rate scenario (the ablation rates are perturbed within their experimental measurement uncertainties to generate the scenarios). The shaded region
945 represents the 68% CI uncertainty envelope of the flow trajectory.

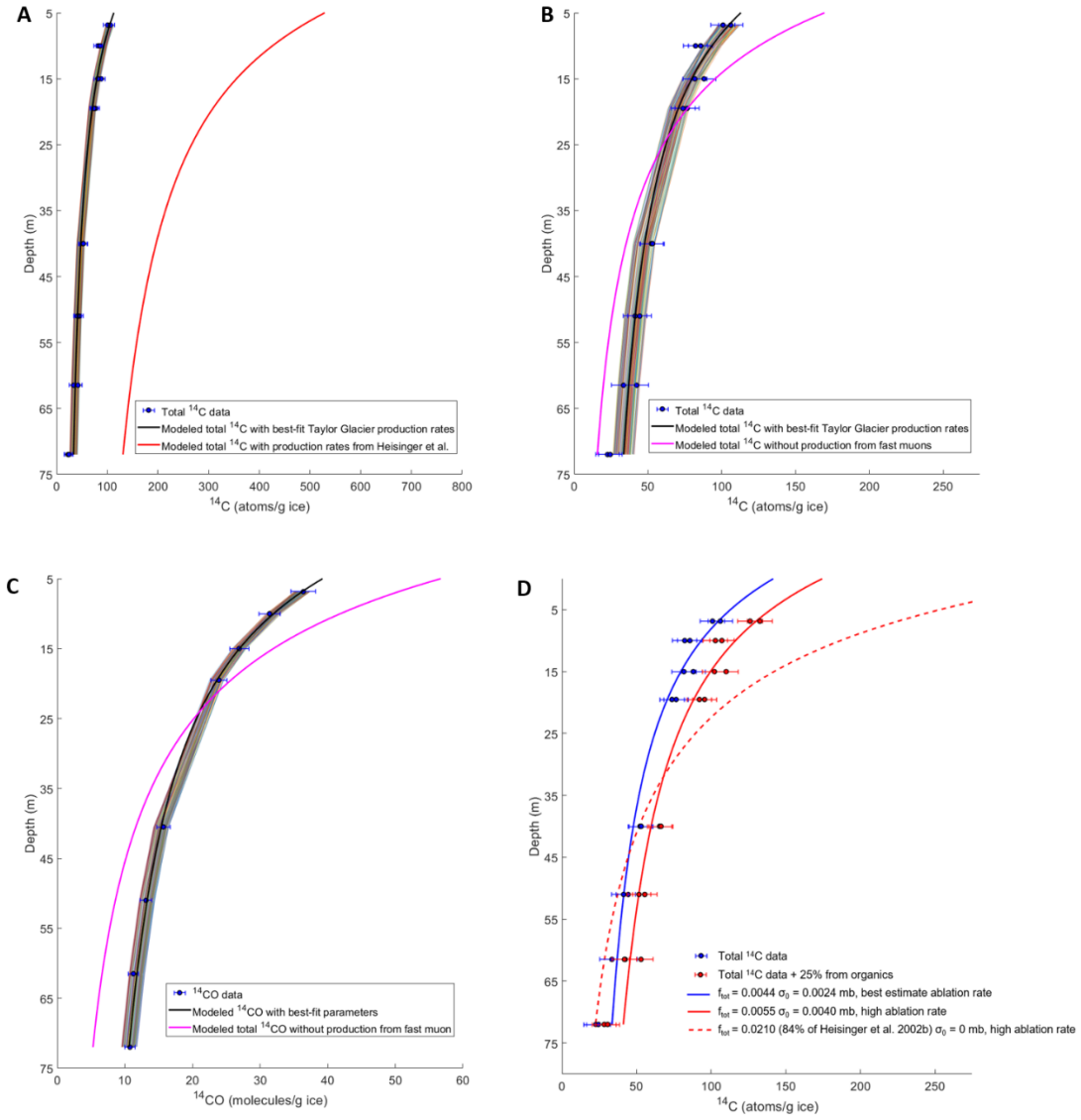

Fig.6. (A). Comparison between total ^{14}C measurements with modeled best-estimate σ_0 and f_{tot} parameters from this study and Heisinger et al. (2002a,b). (B). Comparison between total ^{14}C measurements with modeled best-estimate σ_0 and f_{tot} parameters from this study and modeled total ^{14}C with best-fit f_{tot} when σ_0 is forced to be zero. (C). Comparison between ^{14}CO measurements with modeled best-estimate f_{neg} and f_{fast} parameters from this study and modeled ^{14}CO with best-fit f_{neg} when f_{fast} is forced to be zero. (D). Comparison between total ^{14}C measurements with modeled best-estimate σ_0 and f_{tot} parameters from this study and modeled total ^{14}C from the sensitivity analyses when we assume 25% contribution from organics and high ablation rate scenario (Fig. S9). The thin colored lines represent the 95% CI envelope of the model results (corresponding to the contour plot of Fig. 7A for Fig. 6A and 6B, and contour plot of Fig. 7B for Fig. 6C). The error bars shown on the data are 95% CI. In Fig. 6D, the solid blue line represents the ^{14}C profile from modeled best-estimate f_{tot} and σ_0 under best-estimate ablation rate. The solid red line represents the ^{14}C profile from the sensitivity analysis when f_{tot} and σ_0 are tuned to fit the total ^{14}C data that is scaled by 25% to account for contribution from organics (red dots) under high ablation rate scenario (Fig. S9). The dashed red line represents the ^{14}C profile from the sensitivity

analysis when f_{tot} is kept constant at 0.021 (which is the minimum value provided by Heisinger et al. 2002b) and $\sigma_0 = 0$ (which provides the best-fit against the data).

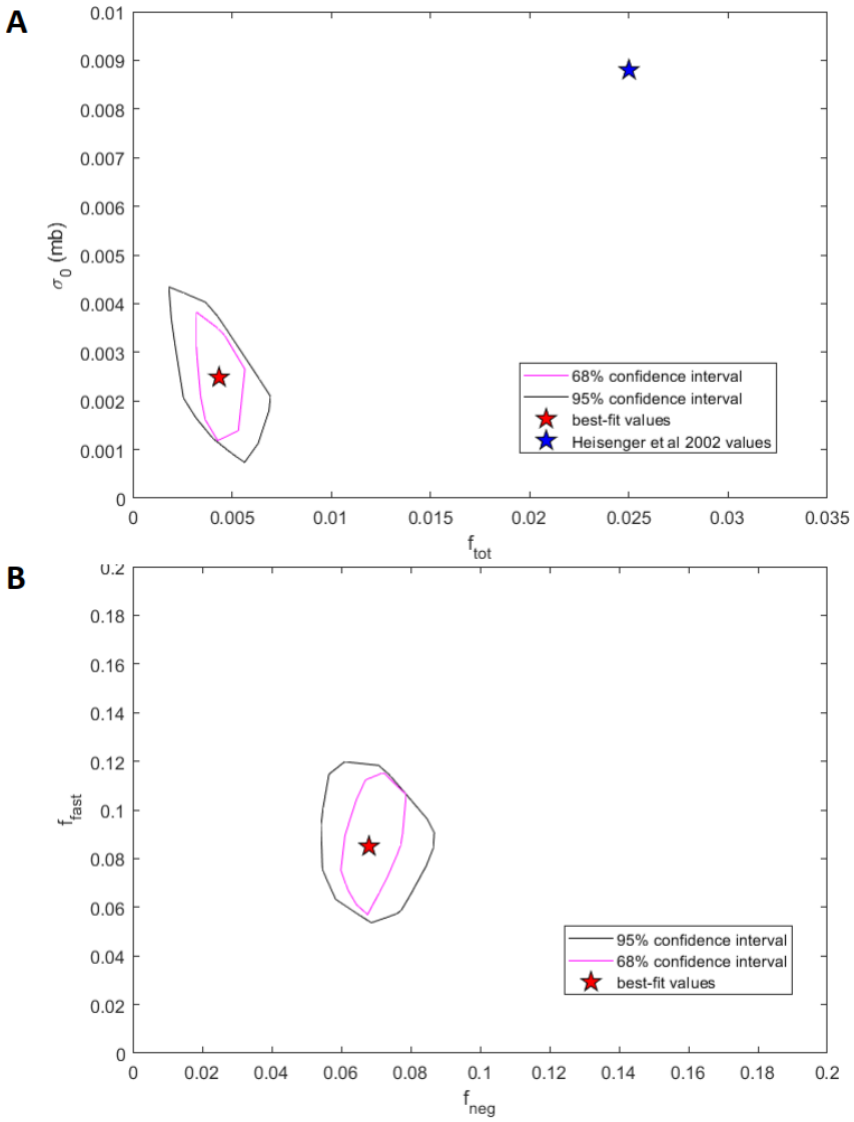

Fig.7. (A). 68% and 95% CI contours of accepted σ_0 and f_{tot} values for total ^{14}C. (B) 68% and 95% CI contours of accepted f_{neg} and f_{fast} values for ^{14}CO (see Section 5.4.3). For comparison, the σ_0 and f_{tot} values from Heisinger et al. (2002a, 2002b) are shown as a blue star. The best-fit values for σ_0, f_{tot}, f_{neg}, and f_{fast} are shown as a red star star in both figures.

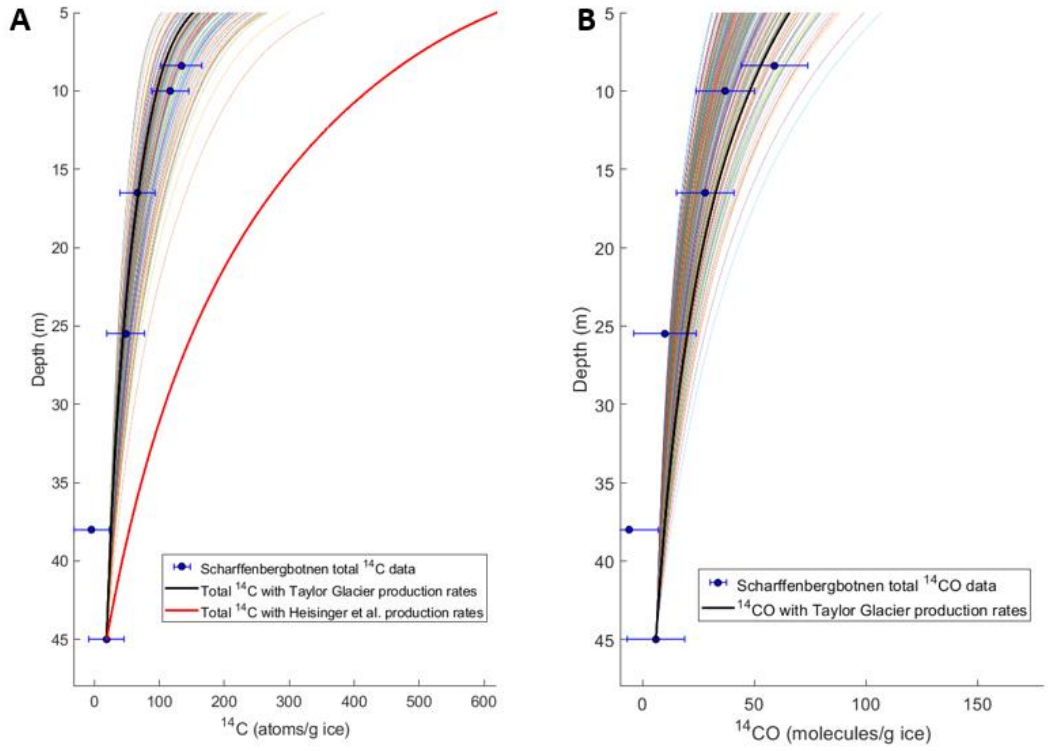

Fig. 8. A. Comparison between measured total ^{14}C from Scharffenbergbotnen, expected total ^{14}C using production rates inferred in this study, and expected total ^{14}C using Heisinger et al. (2002a, 2002b) production rates. B. Comparison between measured ^{14}CO from Scharffenbergbotnen and expected ^{14}CO using production rates inferred from Taylor Glacier. The colored lines on both figures represent the 95% CI envelope of the model results. At the depths plotted in this figure (deeper than 5m), production from neutron-induced spallation is negligible.

Table 1. Measured $^{14}CO_2$, ^{14}CO, $^{14}CH_4$ after all associated corrections and calculated total ^{14}C, $^{14}CH_4/^{14}CO$ ratios, $^{14}CO_2$ and ^{14}CO fractions. The data from Petrenko et al. (2016) are marked with asterisks (*). All errors presented indicate the 95% CI.

Mid-depth *(m)*	$^{14}CO_2$ *(molec/g ice)*	^{14}CO *(molec/g ice)*	$^{14}CH_4$ *(molec/g ice)*	Total ^{14}C *(atoms/g ice)*	$^{14}CH_4/^{14}CO$ ratio	$^{14}CO_2$ fraction	^{14}CO fraction
2.25	145.5 ± 32.0	45.2 ± 3.2*	0.418 ± 0.052*	191.1 ± 32.2	0.0092 ±0.0013	0.76 ±0.18	0.24 ±0.04
	123.3 ± 28.5			168.9 ± 28.7		0.73 ±0.18	0.27 ±0.05
3.65	88.5 ± 7.8	41.9 ± 2.2*	0.327 ± 0.026*	130.7 ± 8.1	0.0078 ±0.0007	0.68 ±0.07	0.32 ±0.03
	98.0 ± 7.8			140.2 ± 8.1		0.70 ±0.07	0.30 ±0.02
6.85	64.2 ± 7.8	36.4 ± 1.8*	0.273 ± 0.020*	100.9 ± 8.0	0.0075 ±0.0007	0.64 ±0.08	0.36 ±0.03
	69.4 ± 7.8			106.1 ± 8.0		0.65 ±0.08	0.34 ±0.03
10**	50.6 ± 7.8	31.4 ± 1.6*	N/A	82.2 ± 8.0**	N/A	0.62 ±0.10	0.38±0.04
	54.3 ± 7.8			86 ± 7.9**		0.63 ±0.10	0.37±0.04
15	60.9 ± 7.8	26.9 ± 1.4*	0.206 ± 0.016*	88.0 ± 7.9	0.0077 ±0.0007	0.69 ±0.10	0.31 ±0.03
	54.6 ± 7.8			81.7 ± 7.9		0.67 ±0.10	0.33 ±0.04
19.5	52.4 ± 7.8	23.9 ± 1.2*	0.182 ± 0.016*	76.5 ± 7.9	0.0076 ±0.0008	0.69 ±0.11	0.31 ±0.04
	49.6 ± 7.8			73.7 ± 7.9		0.67 ±0.11	0.32 ±0.04
40.5	36.4 ± 7.8	15.8 ± 1.0	0.119 ±0.013	52.3 ± 7.8	0.0075 ±0.0010	0.70 ±0.15	0.30 ±0.05
	37.2 ± 7.8			53.1 ± 7.9		0.70 ±0.15	0.30 ±0.05
51	31.1 ± 7.8	13.2 ± 0.9	0.097 ±0.014	44.4 ± 7.8	0.0073 ±0.0012	0.70 ±0.18	0.30 ±0.06
	28.0 ± 7.8			41.3 ± 7.8		0.68 ±0.19	0.32 ±0.06
61.5	22.1 ± 7.8	11.3 ± 0.7	0.079 ±0.013	33.5 ± 7.8	0.0070 ±0.0012	0.66 ±0.24	0.34 ±0.08
	31.0 ± 7.8			42.4 ± 7.8		0.73 ±0.19	0.27 ±0.05
72	11.8 ± 7.8	10.8 ± 0.7	0.080 ±0.013	22.7 ± 7.8	0.0074 ±0.0013	0.52 ±0.34	0.48 ±0.17
	13.6 ± 7.8			24.5 ± 7.8		0.55 ±0.32	0.44 ±0.14

**the total 14C value for 10m sample was scaled by a factor of 1.003 ± 0.003 (95% CI) to account for the lack of $^{14}CH_4$ measurements (Section 4.2).

Table 2. Probability of ^{14}C production from stopped negative muons (f_{tot}), reference nuclear reaction cross section for production via fast muon interactions (σ_0), and total ^{14}C production rates in ice at the surface from the two muon reactions rescaled to SLHL (sea level, high latitude) using Lifton et al. (2014) scaling. All errors shown represent 95% confidence intervals.

	Overall probability of negative muon capture reaction (f_{tot})	Reference nuclear reaction cross section (σ_0) (millibarn)	SLHL total ^{14}C production rate in ice by negative muons (atoms g ice^{-1} yr^{-1})	SLHL total ^{14}C production rate in ice by fast muons (atoms g ice^{-1} yr^{-1})
This study	0.0044 (+0.0026/-0.0026)	0.0024 (+0.0017/-0.0018)	0.79 (+0.47/-0.46)	0.21 (+0.16/-0.15)
Heisinger et al. (2002a,b)	0.025 ± 0.004	0.0088 (+0.0098/-0.0088)	4.76 ± 0.76	0.74 (+0.83/-0.74)
Lupker et al. (2015)	0.024 (+0.006/-0.016)*	0 (+0.0118/-0)	4.70 (+1.22/-3.04)	0 (+1.52/-0)

*adjusted to ice assuming the chemical compound factor (f_c) of ice is 1.0 and f_c for quartz is 0.704 (Heisinger et al. 2002b).

Table 3. ^{14}CO-specific surface production rates in ice from the two muon mechanisms normalized to SLHL (sea level, high latitude) site using Lifton et al. (2014) scaling. All errors shown represent 95% confidence intervals.

	SLHL ^{14}CO production rate in ice by negative muons (molec g ice^{-1} yr^{-1})	SLHL ^{14}CO production rate in ice by fast muons (molec g ice^{-1} yr^{-1})
This study	0.310 (+0.075/-0.063)	0.063 (+0.022/-0.018)
Petrenko et al. (2016)	0.24 (+0.14/-0.14)	0.053 (+0.028/-0.028)